nature communications

Article

https://doi.org/10.1038/s41467-024-55187-w

The survival of B cells is compromised in kidney disease

Received: 24 January 2024

Accepted: 4 December 2024

Published online: 30 December 2024

Check for updates

Doureradjou Peroumal[1,2,8], Chetan V. Jawale[1,2,8], Wonseok Choi[1,2,3], Hossein Rahimi[1,2,3], Danielle Antos[2,4], De-dong Li[1,2], Shuxia Wang[1], Godhev K. Manakkat Vijay[2,5], Isha Mehta[2,5], Raymond West[6], Muthusamy Thangaraju[7], Thomas D. Nolin[6], Jishnu Das[2,5], John F. Alcorn[2,4] & Partha S. Biswas[1,2,3]

Antibody-mediated protection against pathogens is crucial to a healthy life. However, the recent SARS-CoV-2 pandemic has shown that pre-existing comorbid conditions including kidney disease account for compromised humoral immunity to infections. Individuals with kidney disease are not only susceptible to infections but also exhibit poor vaccine-induced antibody response. Using multiple mouse models of kidney disease, we demonstrate that renal dysfunction inhibits germinal center (GC) response against T-dependent antigens. GC B cells exhibit increased apoptosis in kidney disease. Uremic toxin hippuric acid drives loss of mitochondrial membrane potential, leading to increased apoptosis of GC B cells in a G-protein–coupled receptor 109A dependent manner. Finally, GC B cells and antibody titer are diminished in mice with kidney disease following influenza virus infection, a major cause of mortality in individuals with renal disorders. These results provide a mechanistic understanding of how renal dysfunction suppresses humoral immunity in patients with kidney disease.

Vaccinations have made enormous contributions to global health by saving millions of lives from deadly infections. In recent years, clinical management of infectious conditions has encountered many new challenges including the coexistence of multiple diseases, also known as comorbidities[1,2]. The pre-existing comorbid conditions not only predispose individuals to infections but also alter immune function and make them more susceptible to infectious agents. Hence, comorbidity is linked to complex clinical management, poor health outcomes, and increased healthcare costs[1,2]. One such comorbid condition associated with an increased risk of severe infections and infection-related hospitalizations and deaths is kidney disease. Infections are the second major cause of mortality (20%) in patients with kidney disease, especially those undergoing renal replacement therapy[3]. Epidemiological data from the recent pandemic revealed that SARS-CoV-2-related mortality was about ten times higher in patients with kidney disease than those with normal renal function[4,5]. With a rise in the incidence of kidney disease (estimated to be 17% of the US adult population in 2019; www.cdc.gov), it is imperative to understand how kidney disease impacts anti-microbial immunity and utilize this knowledge for the development of better therapeutic strategies to control infection-related deaths in these patients.

Following infection or immunization, activated B cells undertake a bifurcated response in the secondary lymphoid organs[6–9]. Some of the B cells rapidly form non-canonical short-lived plasmablasts in the

[1]Division of Rheumatology and Clinical Immunology, Department of Medicine, University of Pittsburgh, Pittsburgh, PA, USA. [2]Department of Immunology, University of Pittsburgh, Pittsburgh, PA, USA. [3]Department of Microbiology and Immunology, Renaissance School of Medicine, Stony Brook University, Stony Brook, NY, USA. [4]Department of Pediatrics, University of Pittsburgh, Pittsburgh, PA, USA. [5]Center for Systems Immunology, Department of Immunology and Computational & Systems Biology, University of Pittsburgh, Pittsburgh, PA, USA. [6]Department of Pharmacy and Therapeutics, University of Pittsburgh, Pittsburgh, PA, USA. [7]Department of Biochemistry and Molecular Biology, Medical College of Georgia, Augusta University, Augusta, GA, USA. [8]These authors contributed equally: Doureradjou Peroumal, Chetan V. Jawale. e-mail: partha.biswas@stonybrook.edu

extrafollicular (EF) space. The activated B cells also enter a canonical pathway where they undergo somatic hypermutation and affinity maturation in germinal centers (GC), a unique dynamic structure that forms during the immune response. The interaction between follicular dendritic cells, T follicular helper cells (TFh), and B cells in the GC ultimately gives rise to long-lived memory B cells and plasma cells; the latter secrete high-affinity antibodies.

Uremia, a clinical condition associated with the worsening of kidney function, is characterized by the accumulation of at least 900 metabolic wastes in the body[10–12]. A subset of these metabolites negatively impacts biological systems and are identified as uremic toxins. Uremic toxins are considered a predisposing factor for infections in kidney disease independent of renal replacement therapy[13–15]. The common notion is that uremic toxins induce some form of immune system aging leading to the high occurrence of infections and inadequate vaccine response, a process that is poorly understood. Indeed, data from observational clinical studies implicated kidney disease with poor antibody response following infection or vaccination[16–19]. However, very little is known about how uremic toxins impact B cell response, which is critical for antibody-mediated protection against infectious disease.

Impaired humoral immunity in kidney disease is linked to reduced B cell survival and proliferation[20–22]. The gradual reduction in the glomerular filtration rate correlated with a decrease in the naïve and memory B cells number, a phenotype attributed to diminished expression of the receptor for the B cell survival factor BAFF[20,23]. In vitro studies showed that increased apoptosis of B cells from kidney disease patients is due to reduced expression of anti-apoptotic factor Bcl2[24]. To date, most studies linking kidney disease with abnormal B cell response were either performed in vitro or were correlative in nature. A recent study showed compromised GC-derived immunity in kidney transplant patients following SARS-CoV-2 mRNA vaccination[25]. Since kidney transplant patients are immune compromised, it is difficult to assess the impact of kidney disease on B cell response per se. The identity of uremic toxins and the mechanisms by which these metabolites impair humoral immunity in vivo are largely unexplored.

Individuals with kidney disease show a defect in the immune response against influenza virus infection[26,27]. Hence, these patients are at a higher risk of developing more severe influenza complications, which result in increased hospitalizations and even deaths. Moreover, patients with kidney disease require a higher dose of influenza vaccine to generate protective immunity than healthy individuals[28]. B cells play a key role in immunity to influenza virus during primary and secondary infections[29]. However, no in vivo studies have assessed the impact of kidney disease on B cell function against clinically relevant pathogens.

Using multiple mouse models of kidney disease, we systematically assess B cell responses to a T-dependent model antigen, NP-KLH, and influenza infection. Our data show that kidney dysfunction inhibits GC responses following NP-KLH immunization. B cells from mice with kidney disease exhibit increased apoptosis in GC. We discover that the uremic toxin hippuric acid activates G-protein–coupled receptor 109A (GPR109A), leading to the loss of mitochondrial membrane potential and increased apoptosis in GC B cells. Furthermore, GC B cells, T follicular helper cells, and influenza-specific antibody titers are diminished in mice with kidney disease following viral infection. These findings provide mechanistic insights into how hippuric acid inhibits humoral immunity in kidney disease, which is critical for protection against infectious conditions.

Results

Mice with kidney disease show defects in GC and antibody response

To define how B cells respond in kidney disease, we utilized a clinically relevant mouse model of chemically induced acute kidney disease (Aristolochic acid nephropathy or AAN), as described before[30–34]. Briefly, C57BL/6 (WT) mice were either intra-peritoneally (i.p.) injected with a single dose of nephrotoxin Aristolochic acid I (AAI), AAII (chemical control for AAI) or PBS (control). Both AAI and AAII are the main components of the *Aristolochia* and *Asarum spp*. of plants and exhibit similar mutagenic and genotoxic properties due to their ability to form covalent DNA adducts. The molecular structures of AAI and AAII differ by only one methoxy group, which may have important implications for their toxic effects on kidney epithelial cells. Consequently, mice injected with AAI but not AAII develop renal fibrosis and kidney dysfunction, as evidenced by elevated concentrations of serum blood urea nitrogen (BUN) and uremic toxins[31,32,35].

AAN and control mice were i.p. immunized with a T-dependent model antigen NP-KLH in alum four days after AAI injection, a time point at which AAN mice start developing kidney disease and uremia (Fig. 1A and Fig. S1A, B)[30]. The mice were assessed for B cell response in the spleen at day 12 post-immunization. AAN mice demonstrated a highly variable but comparable number of B cells in the spleen and bone marrow at day 12 post-immunization (Fig. 1B and Fig. S1C). Interestingly, flow cytometry analysis revealed a marked reduction in the percentage and absolute number of total and NP-specific GC B cells in the AAN spleen and renal lymph nodes (Fig. 1C, D and Fig. S1D). Immunofluorescence staining of spleen sections confirmed smaller GC within the B cell follicles in AAN mice (Fig. 1E). There was no difference in the size of GC between control or AAII-injected spleens. Moreover, AAN mice showed reduced GC response at day 21 post-immunization, indicating that GC formation was indeed diminished and not delayed in kidney disease (Fig. S1E). We observed a negative correlation between the serum BUN level and the percentage of GC B cells in AAN mice at day 12 post-immunization (Fig. S1F). These results indicate that GC formation is impaired in kidney disease during T-dependent immune response.

Impaired isotype switching, affinity maturation, TFh generation, and secondary B cell response in kidney disease

The GCs are important sites for isotype switching and affinity maturation during immune response[6,7]. AAN mice exhibited a reduced percentage and absolute number of NP-specific switched $IgG1^+$ B cells than control spleens (Fig. 2A and Fig. S2A). The serum was subjected to ELISA to detect IgG1 specific for high-affinity (NP4 or NP7) and low-affinity (NP27) antigens at days 12 and 21 post-immunization. AAI-injected mice showed diminished NP4 or NP7- but not NP27-specific IgG1 titers in the serum and consequently a lower NP4/NP27 ratio (day 12 post-immunization) and NP7/NP27 ratio (day 21 post-immunization) compared to control mice, reflective of a defective affinity maturation (Fig. 2B–D and Fig. S2B). Consistent with this defect, the ELISPOT assay showed a reduced number of NP4-specific IgG1-producing plasma cells in the spleen of AAI-injected mice (Fig. 2E)[6,7]. The overall diminished B cell response in AAN mice cannot be attributed to increased glucocorticoids due to kidney disease since serum glucocorticoid levels were comparable between the groups (Fig. S2C). These data suggest that GC formation and affinity maturation were compromised in kidney disease.

T-dependent antibody response is initiated and sustained by continuous crosstalk between the activated B and T cells at the boundary of B/T cell zones and within the GC[8]. There was no difference in the frequencies of activated $CD4^+$ and $CD8^+$ T cells between AAN and control groups at day 12 post-immunization (Fig. S2D, E). However, AAN mice demonstrated a diminished percentage and absolute number of TFh cells compared to control spleens (Fig. 2F and Fig. S2F). This was accompanied by an increase in the number of T regulatory (Treg) cells in the AAI-injected mice (Fig. S2G). Several studies showed that the generation of TFh cells is initiated and driven by IL-6 produced by activated B cells[36–41]. Hence, we measured ex vivo IL-6 production from the splenic B cells isolated from immunized AAN and control mice. The B cells purified from the spleen of AAI-injected mice produced

https://doi.org/10.1038/s41467-024-55187-w

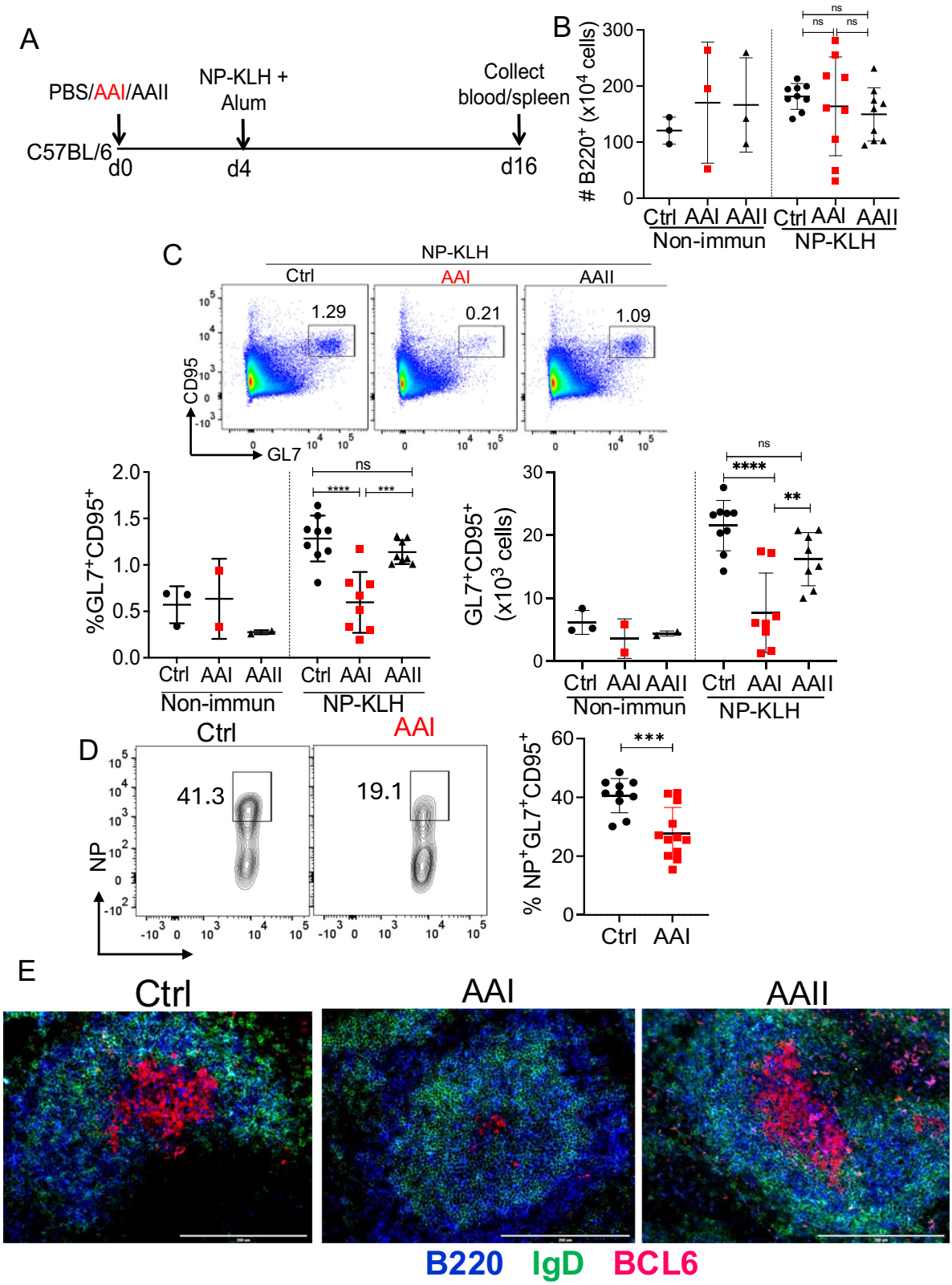

Fig. 1 | Impaired GC formation in AAN mice. A Schematic diagram of the experimental design. C57BL/6 (WT) mice were i.p. injected with a single dose of AAI, AAII (7.5 mg/kg b.wt), or PBS (Ctrl). Mice were either immunized with NP-KLH in alum or left non-immunized 4 days post-AAI injection. At 12 days post-immunization, spleens were assessed for **B** B cells (liveB220$^+$) [Non-immun: Ctrl (3), AAI (3), AAII (3); NP-KLH: Ctrl (9), AAI (9), AAII (9)] **C** total GC B cells (liveB220$^+$GL7$^+$CD95$^+$) [Non-immun: Ctrl (3), AAI (2), AAII (2); NP-KLH: Ctrl (9), AAI (8), AAII (8)], **D** NP-specific GC B cells (liveB220$^+$NP$^+$GL7$^+$CD95$^+$) [NP-KLH: Ctrl (10), AAI (12)] by flow cytometry, and (**E**) GC formation ($n = 3$) by immunofluorescence staining of spleen section. Scale bar = 50 µm. Each dot represents individual mice and data are pooled from at least 2–3 independent experiments (**B**–**D**). Data expressed as Mean ± SD. Statistical analyses by One-way ANOVA (**B**, **C**) and two-sided t-test (**D**). **C** Ctrl vs. AAI ****$P < 0.0001$, AAI vs. AAII ***$P = 0.0007$ and Ctrl vs. AAI ****$P < 0.0001$, AAI vs. AAII **$P = 0.0060$. **D** *** $P = 0.0008$. ns: statistically not significant. Source data are provided as a Source Data file.

https://doi.org/10.1038/s41467-024-55187-w

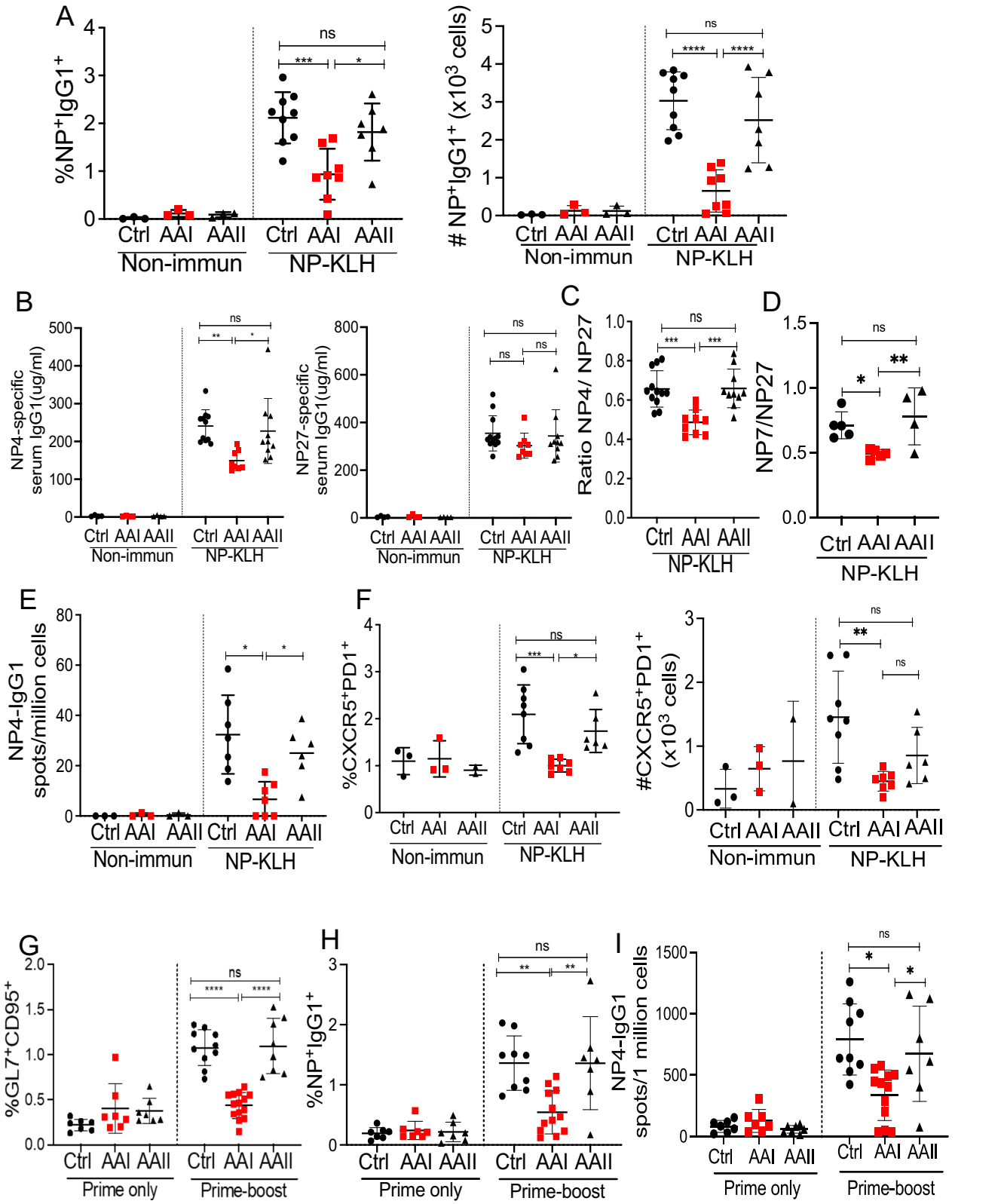

diminished IL-6 than control mice following in vitro LPS stimulation, as assessed by intracellular cytokine staining (Fig. S2H).

We next evaluated secondary B cell response in mice with kidney disease. To achieve this objective, AAI-injected and control mice were primed with NP-KLH in alum followed by a boost with NP-KLH only at day 36 post-immunization. The mice were evaluated for B cell response six days later, a time point at which AAN mice demonstrated kidney dysfunction (Fig. S2I). AAN mice showed diminished secondary total GC formation compared to control mice (Fig. 2G). We also observed diminished NP-specific switched IgG1$^+$ B cells and NP4-specific IgG1-producing plasma cells in the spleen of AAN mice (Fig. 2H, I). Overall, these results suggest that mice with kidney disease show impairment in secondary B cell response following prime-boost immunization.

Fig. 2 | Mice with kidney disease show defects in affinity maturation, TFh, and secondary B cell response. C57BL/6 (WT) mice were i.p. injected with a single dose of AAI, AAII (7.5 mg/kg b.wt), or PBS (Ctrl). Mice were either immunized with NP-KLH in alum or left non-immunized (non-immun) 4 days post-AAI injection. At day 12 post-immunization, spleens were assessed for **A** NP-specific switched IgG1$^+$ B cells (liveIgD$^-$IgM$^-$CD138$^-$Gr1$^-$B220$^+$NP$^+$IgG1$^+$) by flow cytometry [Non-immun: Ctrl (3), AAI (3), AAII (3); NP-KLH: Ctrl (9), AAI (8), AAII (7)], **B** serum NP4 and NP27-specific IgG1 by ELISA [Non-immun: Ctrl (4), AAI (4), AAII (4); NP-KLH Ctrl (12), AAI (8), AAII (10)], and **C** NP4/NP27-specific IgG1 ratio was determined to measure antibody affinity maturation at day 12 post-immunization [NP-KLH: Ctrl (12), AAI (8), AAII (10)]. **D** NP7/NP27-specific IgG1 ratio was determined to measure antibody affinity maturation at day 21 post-immunization [NP-KLH: Ctrl (5), AAI (5), AAII (4)]. **E** NP4-specific antibody-secreting plasma cells generation in the spleen by ELISPOT assay [Non-immun: Ctrl (3), AAI (3), AAII (3); NP-KLH: Ctrl (7), AAI (7), AAII (6)]. **F** The frequency of TFh (liveCD4$^+$CD44$^+$CXCR5$^+$PD1$^+$) cells in the spleen was determined by flow cytometry at day 12 post-immunization [Non-immun: Ctrl (3), AAI (3), AAII (2); NP-KLH: Ctrl (8), AAI (7), AAII (6)]. AAN and control mice were primed with NP-KLH in alum followed by NP-KLH boost 36 days later. Primed only and boosted mice spleens were evaluated for **G** total GC (liveB220$^+$GL7$^+$CD95$^+$) [Prime only: Ctrl (7), AAI (7), AAII (7); Prime-boost: Ctrl (10), AAI (14), AAII (8)], **H** NP-specific switched IgG1$^+$ B cells (liveIgD$^-$IgM$^-$CD138$^-$ Gr1$^-$B220$^+$NP$^+$IgG1$^+$) [Prime only: Ctrl (7), AAI (7), AAII (7); Prime-boost: Ctrl (9), AAI (12), AAII (7)], and **I** NP4-specific IgG1-producing plasma cells 6 days later [Prime only: Ctrl (7), AAI (7), AAII (7); Prime-boost: Ctrl (9), AAI (12), AAII (7)]. Each dot represents individual mice and data are pooled from at least 2–3 independent experiments (**A**–**I**). Data expressed as Mean ± SD. Statistical analyses by One-way ANOVA (**A**–**I**). **A** Ctrl vs. AAI ***$P = 0.0007$, AAI vs. AAII *$P = 0.0252$ and Ctrl vs. AAI ****$P < 0.0001$, AAI vs. AAII ****$P < 0.0001$. **B** Ctrl vs. AAI **$P = 0.0069$, AAI vs. AAII *$P = 0.0247$. **C** Ctrl vs. AAI ***$P = 0.0004$, AAI vs. AAII ***$P = 0.0005$. **D** Ctrl vs. AAI *$P = 0.0565$, AAI vs. AAII **$P = 0.0063$. **E** Ctrl vs. AAI *$P = 0.020$, AAI vs. AAII *$P = 0.0299$. **F** Ctrl vs. AAI ***$P = 0.0007$, AAI vs. AAII *$P = 0.0276$ and Ctrl vs. AAI **$P = 0.0038$. **G** Ctrl vs. AAI ****$P < 0.0001$, AAI vs. AAII ****$P < 0.0001$. **H** Ctrl vs. AAI **$P = 0.0038$, AAI vs. AAII **$P = 0.0073$. **I** Ctrl vs. AAI *$P = 0.036$, AAI vs. AAII *$P = 0.0492$. ns: statistically not significant. Source data are provided as a Source Data file.

Kidney dysfunction and not nephrotoxin impair GC formation and antibody response

To confirm the negative impact of kidney disease on B cell response (Fig. 1), we measured GC formation in AAN and control mice to another T-dependent antigen [2.5% antigen sheep red blood cells (SRBC)] (Fig. 3A and Fig. S3A, B). In line with the NP-KLH immunization, mice with kidney disease showed impaired GC and TFh cell formation following 2.5% SRBC injection (Fig. 3B, C).

To rule out the possibility of a direct effect of AAI on B cells, NP-KLH immunized AAN and control mice were treated with probenecid, an organic anion transporter inhibitor that prevents damage to kidney tubular epithelial cells and minimizes uremic toxin accumulation without neutralizing AAI, as shown before (Fig. S3C, D)[30,35]. Interestingly, probenecid treatment of AAI-injected mice prevented the defect in GC and TFh cell generation (Fig. 3D, E). Moreover, probenecid-treated AAN mice showed an increased number of NP-specific switched IgG1$^+$ B cells and NP4-specific serum IgG1 titer than untreated AAN mice, arguing against a direct effect of AAI on B cell response (Fig. 3F, G). To rule out the direct impact of AAI-induced kidney inflammation on B cell response, control, and AAN mice were immunized with NP-KLH ten days post-AAI injection. AAN mice showed a similar reduction in total and NP-specific GC response than control when immunized at a gap of ten days (Fig. S3E).

As an independent approach to confirm the role of kidney dysfunction in impaired B cell response, we assessed GC formation in a surgically induced mouse model of kidney disease following NP-KLH immunization. The model of 5/6 nephrectomy involves excision of the upper and lower poles of one kidney followed by nephrectomy of the converse kidney (Fig. 3H), as previously described[30]. The kidneys of 5/6 nephrectomized mice demonstrated extensive fibrosis and dysfunction in comparison to sham-operated animals (Fig. S3F, G). The 5/6 nephrectomized animals exhibited impaired GC, TFh and NP-specific switched IgG1$^+$ B cell generation compared to sham-operated animals (Fig. 3I–K). Consequently, there was reduced serum NP4-specific antibody formation and defect in antibody affinity maturation in 5/6 nephrectomized mice (Fig. 3L, M). There was no difference in the serum glucocorticoid level between 5/6 nephrectomized and sham-nephrectomized mice (Fig. S3H). These data support the notion that compromised B cell response is due to kidney dysfunction and not AAI's impact on the immune system per se.

GC B cells from mice with kidney disease show increased apoptosis

To further understand how uremia impacts GC response, flow-sorted NP-specific GC B cells from kidney disease and control mice were subjected to RNA-Seq analysis (Fig. S4A). The principal component analysis plot demonstrated the variation between GC B cells from kidney disease and control mice as well as the similarity between the sample replicates (Fig. S4B). A number of genes were differentially regulated between the GC of mice with kidney disease and the control spleen (Fig. S4C). Fitting with the diminished GC B cell numbers in renal dysfunction, RNA-seq, and Reactome pathway database analysis revealed the downregulation of multiple cell cycle genes in GC B cells from mice with kidney disease (Fig. 4A, B). Accordingly, there was reduced expression of Ki67, a protein that marks all the cells that have entered the cell cycle, in GC B cells during kidney disease (Fig. 4C and Fig. S4D). Using short-pulsed BrdU labeling, we found that similar proportions of GC B cells from AAN and control mice were in the G2M phase, but significantly fewer uremic cells were in the S phase with an increase in G0-G1 than controls (Fig. 4D). Further, transcriptomic and KEGG pathway analysis revealed upregulation of multiple pro-apoptotic and downregulation of anti-apoptotic genes in the GC B cells of AAN mice (Fig. 4E, F). Consequently, NP-specific but not NP-non-specific GC B cells from AAI-injected mice showed increased active Caspase3 expression than control mice (Fig. 4G).

GC B cells are classified into centrocytes (CD86^{hi}CXCR4^{lo}) and centroblasts (CD86^{lo}CXCR4^{hi}) based on morphologic criteria[6,7]. Within a GC, centrocytes and centroblasts distribute preferentially in a centrocyte-rich light zone (LZ) and a centroblast-rich dark zone (DZ) and migrate extensively between the compartments. Centroblasts undergo vigorous proliferation, somatic hypermutation, and clonal expansion in the DZ[42]. In the LZ, depending on the outcome of BCR and T cell help-based selection, the centrocytes either undergo slow division or apoptosis. Interestingly, several genes identified by transcriptomic analysis to be increased in AAN GC B cells were positive regulators of centrocytes in the LZ (Fig. 4H). On the other hand, control GC B cells exhibited higher expression of genes that positively regulate centroblasts in the DZ (Fig. 4I). While control GC B cells demonstrated the phenotype of centroblasts, AAI-injected total, and NP-specific GC B cells showed increased accumulation in the LZ as centrocytes (Fig. 4J). Taken together, these results highlight a critical role for kidney dysfunction in cell cycle arrest, increased apoptosis, and impaired migratory capabilities of GC B cells.

Hippuric acid drives the loss of mitochondrial membrane potential and increased apoptosis of B cells

We next sought to define the mechanisms by which uremia contributes to increased apoptosis of GC B cells. Our transcriptomic analysis showed upregulation of multiple genes in AAN GC B cells related to loss of mitochondrial membrane potential (Fig. 5A). The loss of mitochondrial membrane potential and enhanced mitochondrial ROS production are the cell-intrinsic factors of apoptosis[43]. TMRE staining of total GC B cells demonstrated increased loss of mitochondrial membrane potential in mice with kidney dysfunction (Fig. 5B and

https://doi.org/10.1038/s41467-024-55187-w

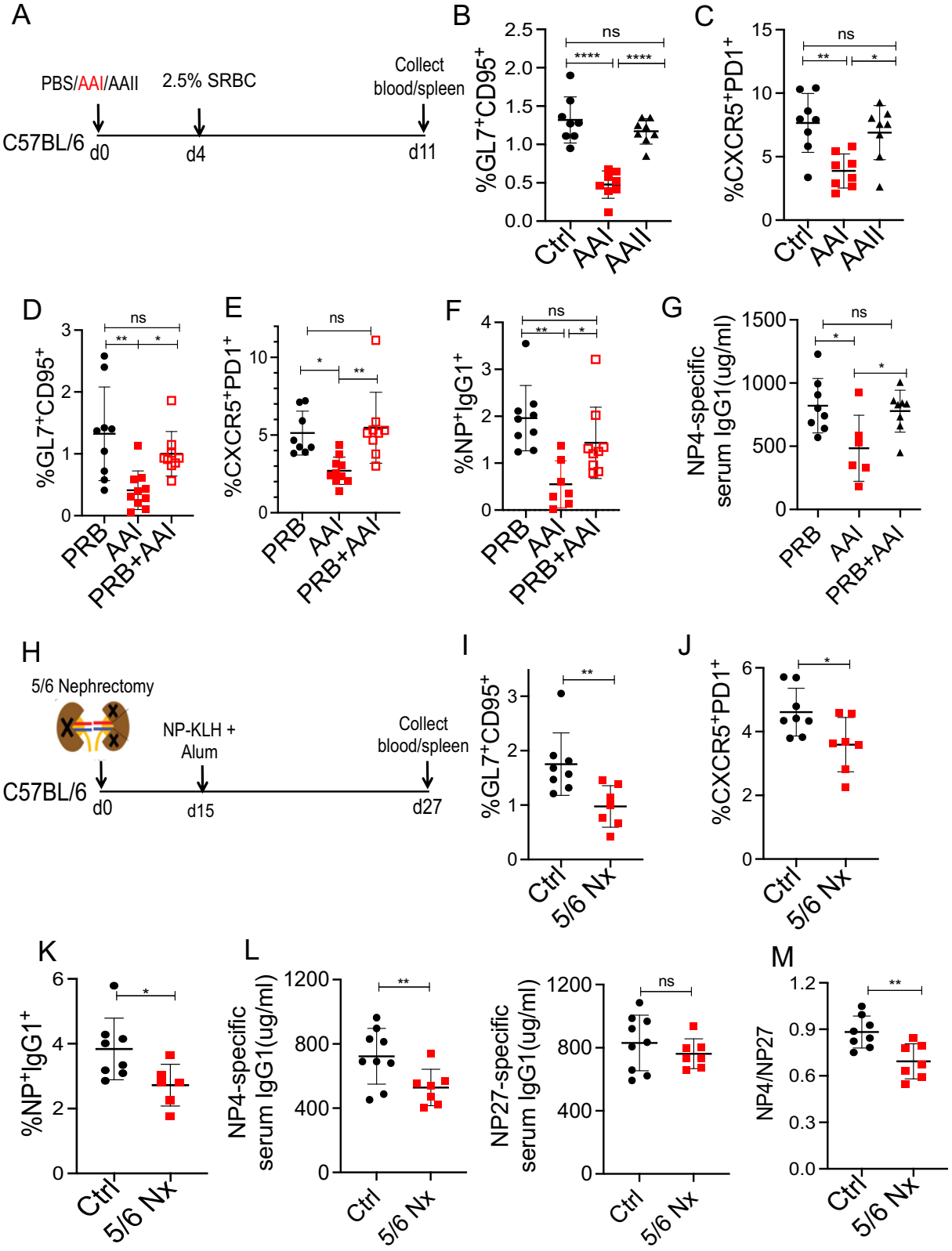

Fig. S5A). GC B cells from AAI-injected mice also exhibited a moderate increase in mitochondrial ROS production (Fig. 5C and Fig. S5B). These results indicate an essential role of kidney disease in causing loss of mitochondrial membrane potential in GC B cells.

A previous study has described an in vitro system in which mouse naïve B cells undergo massive expansion and isotype switching and generate GC-like B cells[44]. Although this is a unique and useful system for studying various aspects of GC biology, it truly does not depict in vivo GC reactions within the secondary lymphoid organs. To identify uremic toxin(s), previously linked to immune dysfunction in uremic patients, that could directly inhibit T cell-dependent B cell response, we utilized an in vitro system for B cell activation and their differentiation into plasmablasts[45–48]. We note that AAN mice also showed a reduced number of extrafollicular plasmablasts (day 4 post-

Fig. 3 | Kidney disease inhibits B cell response during T-dependent immunization. A Schematic diagram of the experimental plan. AAN and control mice were i.p. immunized with 2.5% SRBC ($n = 8$) 4 days post-AAI injection. Seven days later, **B** total GC (liveB220$^+$GL7$^+$CD95$^+$) [SRBC: Ctrl (8), AAI (8), AAII (8)], and **C** TFh (liveCD4$^+$CD44$^+$CXCR5$^+$PD1$^+$) cells were measured by flow cytometry [SRBC: Ctrl (8), AAI (8), AAII (8)]. AAN mice were either treated with probenecid (PRB + AAI) once on day 0 (relative to AAI injection) or left untreated. Control mice received probenecid only (PRB). Four days later, mice received NP-KLH immunization and assessed for **D** total GC B cells [PRB (9), AAI (7), PRB + AAI (9)], **E** TFh cells [PRB (9), AAI (10), PRB + AAI (9)], **F** NP-specific switched IgG1$^+$ B cells (liveIgD$^-$IgM$^-$CD138$^-$ Gr1$^-$B220$^+$ NP$^+$IgG1$^+$) by flow cytometry [PRB (9), AAI (7), PRB + AAI (9)], and **G** serum NP4-specific IgG1 level by ELISA [PRB (8), AAI (6), PRB + AAI (8)]. **H** Diagram of the experimental design. WT mice were either subjected to 5/6 nephrectomy (5/6 Nx) ($n = 7$) or sham-operated (Ctrl) ($n = 8$). Two weeks after surgery, mice were immunized with NP-KLH and assessed for **I** total GC [Ctrl (8), 5/6 Nx (7)], **J** TFh cells [Ctrl (8), 5/6 Nx (7)], **K** NP-specific switched IgG1$^+$ B cells [Ctrl (8), 5/6 Nx (6)], **L** serum NP4 and NP27-specific IgG1 levels [Ctrl (8), 5/6 Nx (7)], and **M** NP4/NP27-IgG1 ratio to measure affinity maturation [Ctrl (8), 5/6 Nx (7)]. Each dot represents individual mice and data are pooled from at least 2–3 independent experiments (**B**–**G** and **I**–**M**). Data expressed as Mean ± SD. Statistical analyses by One-way ANOVA (**B**–**G**) and two-sided t-test (**I**–**M**). **B** Ctrl vs. AAI **** $P < 0.0001$, AAI vs. AAII ****$P < 0.0001$. **C** Ctrl vs. AAI **$P = 0.0027$, AAI vs. AAII *$P = 0.0160$. **D** PRB vs. AAI **$P = 0.0018$, AAI vs. PRB + AAI *$P = 0.0472$. **E** PRB vs. AAI *$P = 0.0112$, AAI vs. PRB + AAI **$P = 0.0029$. **F** PRB vs. AAI **$P = 0.0012$, AAI vs. PRB + AAI *$P = 0.0415$. **G** PRB vs. AAI * $P = 0.0222$, AAI vs. PRB + AAI *$P = 0.0484$. **I** **$P = 0.0096$. **J** *$P = 0.0278$. **K** *$P = 0.0295$. **L** **$P = 0.0028$. **M** **$P = 0.0049$. ns: statistically not significant. Source data are provided as a Source Data file.

immunization) than control mice and lower serum titers of NP27-specific (low affinity) IgM (Fig. S5C, D). The resting splenic B cells were in vitro stimulated with αIgM/αCD40/IL-21 in the presence or absence of different uremic toxins (Fig. 5D). The uremic toxins were added to the culture at concentrations seen in patients with stage 4 and 5 kidney diseases[12]. The cells were assessed for plasmablast (liveB220$^+$CD138$^+$ cells) differentiation by flow cytometry at 4 days post-stimulation (Fig. S5E). Out of total of 9 uremic metabolites tested, only γ-guanidino butyric acid (GBA), indole-3-acetic acid (IAA), para-cresol (PC), para-cresol sulfate (PCS), hippuric acid (HA) and urea (as control) inhibited plasmablast differentiation (Fig. 5E). Since PC is rapidly converted to PCS under in vivo conditions, we have used PCS instead of PC for subsequent experiments.

We selected the above-mentioned five uremic toxins and individually assessed their ability to negatively impact plasmablast proliferation and apoptosis. None of the five toxins inhibited plasmablast proliferation (Fig. 5F and Fig. S5F). Interestingly, only HA showed two-fold higher apoptosis of plasmablasts (Fig. 5G and S5G). The plasmablasts exhibited an increased loss of mitochondrial membrane potential in the presence of HA (Fig. 5H). NP-KLH immunized AAN mice demonstrated an elevated concentration of serum HA (mean value of serum HA is ~35 µg/ml) than control animals at day 12 post-immunization (Fig. 5I). Resting splenic B cells stimulated with αIgM/αCD40/IL-21 in the presence or absence of 35 µg/ml of HA showed increased loss of mitochondrial membrane potential in plasmablasts than untreated control (Fig. 5J). Collectively, these results identify HA as one of the potential uremic toxins in driving the loss of mitochondrial membrane potential and increased apoptosis of B cells during kidney dysfunction.

HA drives GC B cell apoptosis via GPR109A

A recent study showed that HA binds to GPR109A (encoded by *Niacr1* aka *Hcar2 gene*) in osteoclasts and regulates osteoclastogenesis and bone resorption in mice[49]. GPR109A (aka niacin receptor 1) is a high-affinity GPCR for niacin and gut microbes-derived butyrate and β-hydroxybutyrate[50,51]. The GPR109A signaling has been extensively studied in lipolysis, atherogenesis, and intestinal homeostasis[50,51]. However, nothing is known about the role of GPR109A in B cells. The RT-qPCR analysis revealed that resting and αIgM/αCD40/IL-21 or lipopolysaccharide (LPS) activated splenic B cells express comparable levels of *Niacr1* mRNA (Figs. 6A, S6A, B), which was lower than total splenocytes from WT mice. Moreover, FACS-sorted GC (liveB220$^+$GL7$^+$CD95$^+$), non-GC (liveB220$^+$GL7$^-$CD95$^-$), and total splenocytes from NP-KLH immunized WT mice showed *Niacr1* transcript expression at day 12 post-immunization (Figs. 6B, S6C, D). NP-KLH immunized *Niacr1*$^{-/-}$ mice served as a negative control. Intriguingly, GPR109A is not expressed in naïve human B cells isolated from blood (Fig. S6E). In contrast to mouse B cells, the GPR109A expression is upregulated in human B cells following in vitro stimulation with αIgM/sCD40L/IL-21 with the highest expression seen in the plasmablasts.

Next, to define the role of HA/GPR109A signaling in GC B cell apoptosis, purified total splenic WT B cells from NP-KLH immunized mice were in vitro incubated with HA for 6 h and assessed for loss of mitochondrial membrane potential. In vitro, HA treatment diminished GC B cell number and induced increased loss of membrane potential in GC B cells, as evidenced by TMRE staining (Fig. 6C).

To analyze the function of GPR109A stimulation during B cell activation, αIgM/αCD40/IL-21 stimulated B cells were incubated in the presence or absence of two different GPR109A agonists [GSK256073 and Monomethyl fumarate (MMF)][52,53]. Interestingly, treatment with GPR109A agonists showed loss of mitochondrial membrane potential and increased apoptosis of plasmablasts in a dose-dependent manner (Fig. 6D–F and Fig. S6F).

Moreover, to assess the impact of GPR109A activation on GC B cells under in vivo conditions, mice were either treated with MMF or left untreated and then assessed for B cell response following immunization. MMF treatment diminished the number of total and NP-specific GC B cells and impaired affinity maturation (Fig. 6G–I). MMF-treated mice exhibited increased loss of mitochondrial membrane potential in GC B cells than the untreated group (Fig. 6J).

To further confirm that HA drives loss of mitochondrial membrane potential in B cells via GPR109A, αIgM/αCD40/IL-21 stimulated splenic B cells from WT and *Niacr1*$^{-/-}$ mice were cultured in the presence or absence of HA and evaluated for the loss of mitochondrial membrane potential at 24 h post-stimulation. HA-induced loss of mitochondrial membrane potential in WT plasmablasts, a phenotype reversed in the absence of GPR109A in B cells (Fig. 6K). Collectively, these data indicate that HA-mediated activation of GPR109A contributes to the loss of mitochondrial membrane potential in B cells.

B cell-specific GPR109A expression limits humoral immune response in kidney disease

To test the function of GPR109A in impairing GC B cell response in the context of kidney disease, WT, and *Niacr1*$^{-/-}$ mice were subjected to AAN and assessed for B cell response following NP-KLH immunization (Fig. 7A). WT and *Niacr1*$^{-/-}$ mice demonstrated comparable kidney dysfunction following AAI injection (Fig. S7A). Both WT and *Niacr1*$^{-/-}$ mice showed a similar percentage of the total and NP-specific GC B cells and antibody affinity maturation, indicating that GPR109A is dispensable for GC formation and affinity maturation in the control spleen (Fig. 7B–D). As expected, WT mice subjected to AAN showed a reduced number of GC B cells and a defect in affinity maturation. However, AAI-injected *Niacr1*$^{-/-}$ mice showed no impairment in their GC response, as evidenced by a comparable percentage of total and NP-specific GC B cells and antibody affinity maturation.

To define the role of B cell-specific GPR109A in impaired GC response, we adoptively transferred resting splenic B cells from WT or *Niacr1*$^{-/-}$ mice in control or AAI-injected B cell-deficient µMT mice and assessed for GC response after NP-KLH immunization (Fig. 7E). The recipient µMT mice subjected to AAN and receiving either WT or

https://doi.org/10.1038/s41467-024-55187-w

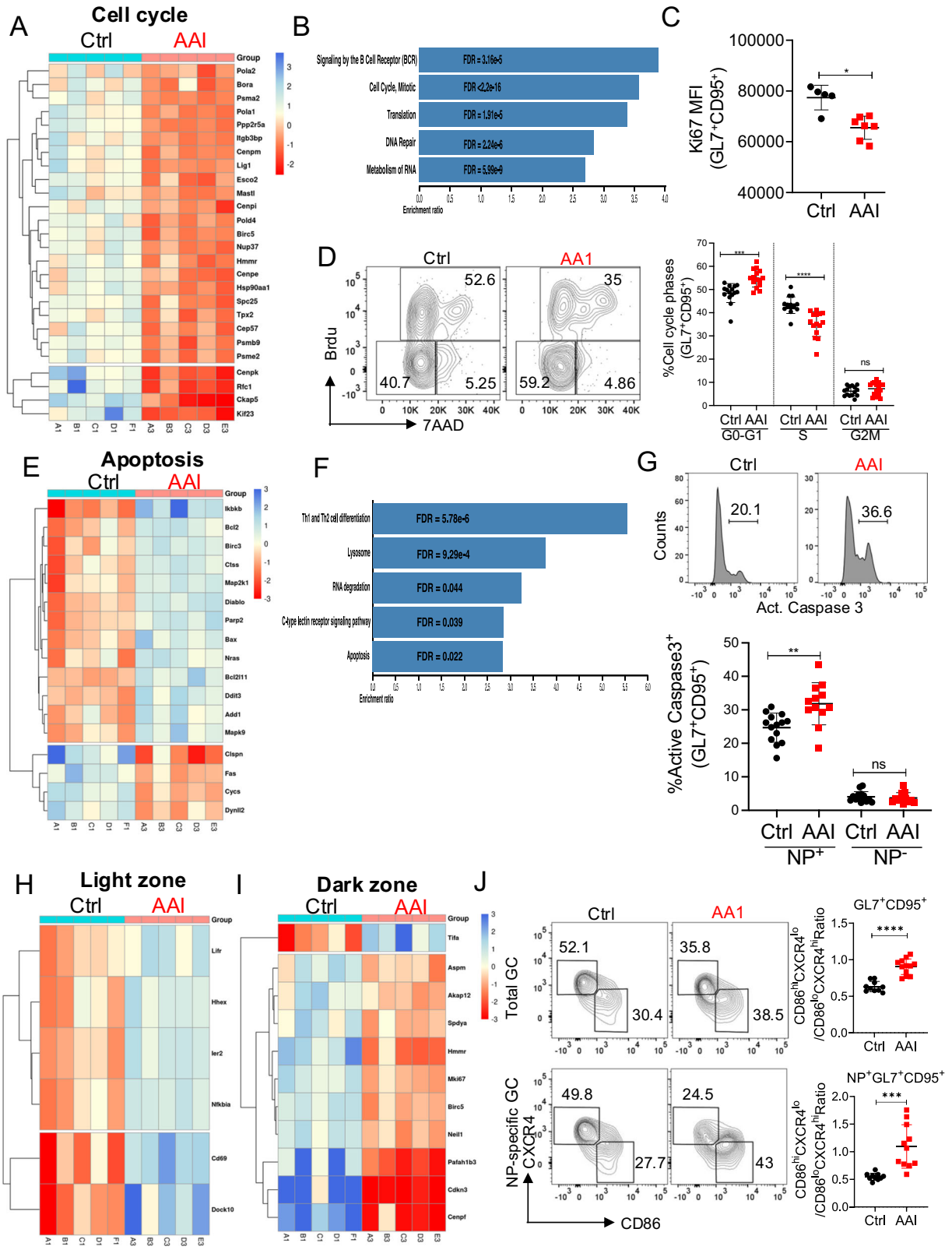

Niacr1$^{-/-}$ B cells showed comparable serum BUN level at day 12 post-immunization (Fig. S7B). As expected, μMT mice with kidney disease and receiving WT B cells showed reduced total and NP-specific GC response compared to control μMT spleen (Fig. 7F, G, Fig. S7C). Interestingly, there was no difference in the percentages and absolute numbers of total and NP-specific GC B cells between control and AAN μMT mice receiving *Niacr1*$^{-/-}$ B cells after NP-KLH immunization. Moreover, Ki67 staining revealed diminished proliferation of WT total GC B cells in AAN μMT mice, an effect abrogated when GC B cells lack *Niacr1* expression (Fig. 7H and Fig. S7D). When evaluated for the loss of mitochondrial membrane potential and mitochondrial ROS generation, *Niacr1*$^{-/-}$ but not WT GC B cells showed no increase in the loss of mitochondrial membrane potential and mitochondrial ROS generation in AAN μMT mice in comparison control recipient (Fig. 7I, J and

Fig. 4 | Kidney dysfunction triggers apoptosis in GC B cells. NP-specific GC B cells from the control and AAN spleen ($n = 5$) were flow sorted on day 12 post-immunization and subjected to RNA-Seq analysis. **A** Relative expression of significantly differentially expressed genes (q-value < 0.05) related to cell cycle, and **B** Over-representation pathway analysis of significantly downregulated genes in AAN GC B cells. **C** MFI of Ki67$^+$ GC B cells [NP-KLH: Ctrl (5), AAI (7)]. **D** Cell cycle status of GC B cells was analyzed at day 12 post-immunization [NP-KLH: Ctrl (15), AAI (15)]. **E** Relative expression of significantly differentially expressed genes (q-value < 0.05) related to apoptosis and **F** Over-representation pathway analysis of upregulated genes in GC B cells from AAN mice. **G** NP$^+$ and NP$^-$ GC B cells staining for active caspase3 expression ($n = 12$–14) at day 12 post-immunization [NP-KLH: Ctrl (14), AAI (12)]. Relative expression of significantly differentially expressed genes (q-value < 0.05) related to **H** Light zone (LZ), and **I** Dark zone (DZ) GC B cells. **J** Number of LZ centrocytes (CXCR4^{lo}CD86^{hi}) and DZ centroblasts (CXCR4^{hi}CD86^{lo}) at day 12 post-immunization [NP-KLH: Ctrl (10), AAI (12)]. Each dot represents individual mice and data pooled from at least 2–3 experiments (**C**, **D**, **G**, and **J**). Data expressed as Mean ± SD. Statistical analyses by two-sided t-test (**C**, **D**, **G**, and **J**). **C** $^*P = 0.0228$. **D** G0-G1 $^{***}P = 0.0001$, S $^{****}P < 0.0001$. **G** $^{**}P = 0.0023$. **J** $^{****}P < 0.0001$ and $^{***}P = 0.0003$. Source data are provided as a Source Data file.

Fig. S7E, F). Consequently, increased Caspase3 activation in NP-specific WT GC B cells was corrected in recipient AAN μMT mice receiving *Niacr1*$^{-/-}$ B cells (Fig. 7K). The recipient AAN μMT mice receiving WT B cells demonstrated a defect in antibody affinity maturation compared to the control recipient, an effect not observed in AAN μMT mice receiving *Niacr1*$^{-/-}$ B cells (Fig. 7L). These data indicate that uremic toxin(s)-mediated activation of GPR109A in B cells is likely responsible for compromised GC response in kidney disease.

Impaired influenza-specific B and T cell responses in uremia

The patients with kidney disease have a higher risk of death from influenza than those with normal kidney function[26,27]. Hence, AAN and control mice have infected with the influenza A virus and assessed for B cell response at 12 days post-infection (p.i) (Fig. 8A). AAI-injected mice showed reduced GC in the spleen than control animals (Fig. 8B). The number of TFh cells in the spleen was also diminished in the AAN mice (Fig. 8C). Accordingly, there was a reduction in the serum anti-PR8HA-specific IgG antibody titer in mice with kidney disease than control animals (Fig. 8D). The inhibitory effect of uremia is not restricted to B cells since AAN mice also exhibited a reduced number of influenza-specific CD8$^+$ T cells (Fig. 8E). These results indicate that kidney dysfunction has a negative impact on influenza-specific B and T cell responses following infection.

To correlate the defect in anti-viral immunity with susceptibility to infection, we compared pulmonary inflammation and viral load between AAN and control mice at day 12 p.i. AAN lungs showed a trend toward diminished peri-vascular, peri-bronchiolar, and parenchymal inflammatory cell influx when compared to control lungs (Fig. 8F). Compromised inflammatory cell infiltration in the AAN lungs resulted in reduced viral clearance, as assessed by qPCR for the M protein gene of the virus (Fig. 8G). Collectively, these results suggest that mice with kidney disease show impaired B and T cell responses leading to uncontrolled viral load in the lungs.

Discussion

Alterations in the immune system that occur with kidney disease are linked to increased susceptibility to infections and inadequate vaccine response[13–15]. On the other hand, chronic immune activation in individuals with kidney disease leads to the progression of inflammatory cardiovascular disease. To date, the majority of the studies focused on understanding the pathogenesis of cardiovascular disease in kidney disease patients, and very little emphasis is placed on defining immune deficiencies that cause fatal infections. Here, we define the impact of uremia on humoral immune response against T-dependent model antigens and influenza virus infection using two distinct mouse models of kidney disease, AAN, and 5/6 nephrectomy. Our studies show that the uremic toxin hippuric acid causes impaired GC response via activation of GPR109A. Efforts directed at mitigating the immune anomalies in kidney disease could potentially lead to a better understanding and, thus, the development of therapies that could reduce the unusually high death rate due to infection in these patients.

Our results show a defect in TFh and influenza-specific CD8$^+$ T cell response in kidney disease, indicating that the inhibitory effect of kidney dysfunction is not limited to B cells. This observation is in line with patients with kidney disease where depletion of naïve and memory T cells is a clinical feature[54,55]. Given the critical role of T cells in anti-microbial immunity, the depletion of these cells must be, in part, responsible for increased susceptibility to infections in kidney disease. However, it is unclear whether diminished T cell function in kidney disease is mediated directly by the uremic toxins or is an outcome of compromised B cell response. We demonstrate that B cells from AAN mice produce less IL-6, required for TFh generation, providing support for the latter theory. The mechanisms of impaired IL-6 production from activated B cells in uremic conditions are unknown. Previous studies have shown the critical role of BCR, anti-CD40, and TLR signaling in IL-6 production from activated B cells. It is unclear how these B cell-intrinsic cell signaling pathways are compromised in uremic conditions. Additionally, B cell-extrinsic signals drive IL-6 production from activated B cells. One such B cell-extrinsic factor is IFNγ, previously shown to induce IL-6 in conjunction with BCR, anti-CD40, and TLR signaling. Hence, it is possible that uremia suppresses IFNγ production in the spleen leading to reduced IL-6 production from activated B cells. Future studies should focus on understanding the impact of various uremic toxin(s) on B cell-intrinsic and extrinsic factors in limiting IL-6 production during immunization. Moreover, the number of activated T cells was not impacted in renal dysfunction, indicating that the defect seen in TFh or virus-specific CD8$^+$ T cell responses cannot be attributed to global immunosuppression. Nevertheless, mechanistic studies delineating the role of kidney dysfunction in shaping various T cell compartments against infections require careful consideration.

Hippuric acid (HA) is produced from the hepatic glycine conjugation of benzoic acid or the gut bacterial metabolism of phenylalanine[56]. Due to a similar structure to niacin, HA binds and activates GPR109A. HA drives osteoclast differentiation and endothelial cell dysfunction in a GPR109A-dependent manner[49,57]. Increased mitochondrial dysfunction plays an active role in HA-induced endothelial cell abnormalities via mitoROS production[57]. We also show that the HA/GPR109A pathway causes loss of mitochondrial membrane potential and increased apoptosis of B cells. Thus, B cell deficiency and dysfunction observed in kidney disease can be simultaneously mediated by HA-induced increased B cell apoptosis and impaired B cell differentiation and maturation. However, we do not rule out the impact of other uremic toxins on compromised B cell response. Future studies should focus on understanding the synergistic and additive effect of HA with other uremic toxins in anti-microbial immunity. Since HA is derived from the gut microbial metabolism of polyphenols to benzoates, the impact of depleting gut microbiota in B cell response in kidney disease warrants detailed investigation.

A previous study was unable to detect GPR109A expression in resting B cells from healthy donors[51]. We also observed no baseline expression of GPR109A in human resting B cells. However, the receptor expression was upregulated following activation, with maximum expression documented on in vitro differentiated plasmablasts. In contrast, mouse resting splenic B cells expressed *Niacr1* mRNA at a level comparable to activated B cells. The reason for this discordance and its functional relevance between human and mouse B cells is presently

https://doi.org/10.1038/s41467-024-55187-w

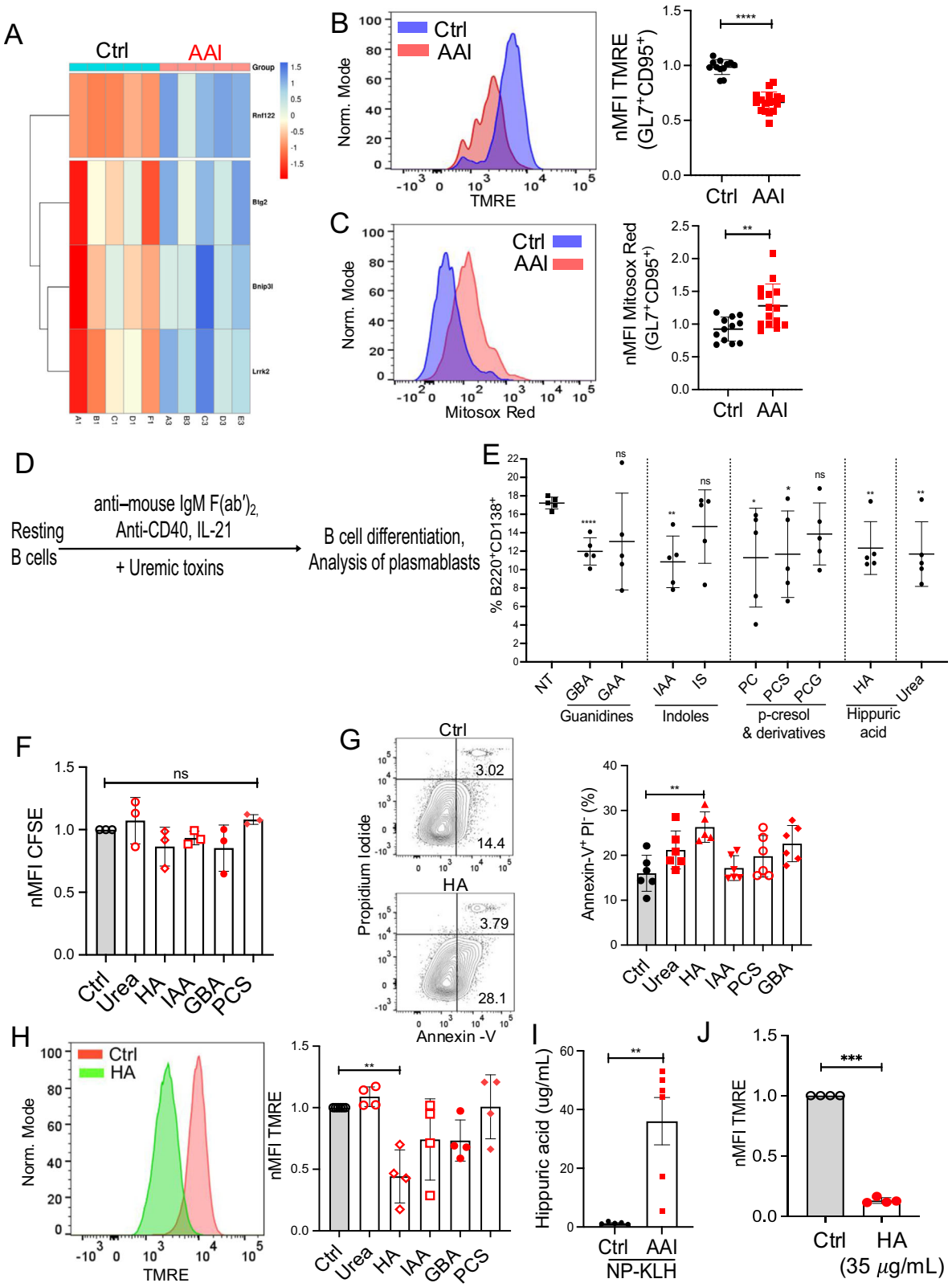

unclear. It is possible that the *Niacr1* gene is differentially regulated in human and mouse B cells, a process that is poorly understood. In the mouse gut, activated GPR109A promotes IgA secretion, indicating that GPR109A signaling is functionally relevant in B cell response[58]. Intriguingly, we did not observe any impact of global GPR109A deletion on GC response in non-uremic mice. These data suggest that niacin and other non-HA ligands-mediated activation of GPR109A are dispensable for GC B cells in mice with normal kidney function.

Additionally, the public domain RNA-seq database (Immgen) failed to detect *Niacr1* transcript expression in GC B cells. It is important to note that, the ImmGen database, which is a cis-regulatory atlas of the mouse immune cells, characterizes germinal center B cells (GC)

Fig. 5 | HA drives loss of mitochondrial membrane potential in B cells. A NP-specific GC B cells from the control and AAN spleen ($n = 5$) were flow sorted on day 12 post-immunization for RNA-Seq analysis. Relative expression of significantly differentially expressed genes (q-value < 0.05) related to mitochondrial membrane potential. At day 12 post-immunization, **B** mitochondrial membrane potential [NP = KLH: Ctrl (12), AAI (17)], and **C** mitoROS production [NP = KLH: Ctrl (12), AAI (15)] were measured in GC B cells by TMRE and MitoSox Red staining, respectively. **D** Schematic diagram of in vitro B cell assay. **E** WT resting splenic B cells ($n = 5$) ± uremic toxins were stimulated with αIgM/αCD40/IL-21 and the number of $B220^{+}CD138^{+}$ plasmablasts was determined by flow cytometry at 96 h. WT B cells ± αIgM/αCD40/IL-21 ± uremic toxins and **F** proliferation (CFSE dilution) of plasmablasts was assessed at 48 h ($n = 3$), **G** apoptosis ($n = 6$), and **H** mitochondrial membrane potential was measured in plasmablasts at 24 h ($n = 4$). **I** HA concentration in the serum of mice was measured by LC-MS/MS [Ctrl (5), AAI (6)]. **J** WT splenic B cells + αIgM/αCD40/IL-21 ± HA (35 μg/ml) were assessed for the loss of mitochondrial membrane potential in plasmablasts at 24 h. Each dot represents individual mice (**B**, **C**, and **I**) and 5 (**E**), 3 (**F**), 6 (**G**), and 4 (**H**, **J**) experiments. Data pooled from 2–3 experiments (**B**, **C**, and **I**). Data expressed as Mean ± SD. Statistical analyses by One-way ANOVA (**E**–**H**) and two-sided t-test (**B**, **C**, **I**, and **J**). **B** ****$P < 0.0001$. **C** **$P = 0.0029$. **E** NT vs. GBA ****$P < 0.0001$, NT vs. IAA **$P = 0.0011$, NT vs. PC *$P = 0.0398$, NT vs. PCS *$P = 0.0307$, NT vs. HA **$P = 0.0059$, NT vs. Urea **$P = 0.0084$. **G** Ctrl vs. HA **$P = 0.0019$. **H** Ctrl vs. HA **$P = 0.0032$. **I** **$P = 0.0037$. **J** ***$P = 0.0004$. ns: statistically not significant. Source data are provided as a Source Data file.

in 5–6 weeks old unimmunized C57BL/6 mice, while we examined GC B cells post NP-KLH/alum immunization[59]. ImmGen uses bulk RNA-seq which has assay false negatives i.e., *Niacr1* may have been missed in GC B cells due to several technical reasons including inadequate read depth. Our assay (RT-qPCR for *Niacr1* mRNA) is more specific and is targeted to detect the presence of *Niacr1* transcript.

Although GPR109A is mostly known for its antilipolytic effects in adipocytes, recent studies suggest that activation of this receptor is associated with cell death pathways. GPR109A activation in mature human neutrophils accelerated apoptosis due to G-inhibitory protein-coupled receptor [G(i)]-mediated inhibition of adenylyl cyclase activity leading to mitochondrial dysfunction, as demonstrated by increased mitochondrial ROS generation[60,61]. Similarly, GPR109A in breast cancer cells diminished cyclic AMP production leading to mitochondrial dysfunction and increased apoptosis[62]. This process also involves downregulation of Bcl2, Bcl-xL, and cyclin D1, and upregulation of the death receptor pathways following GPR109A activation in colon cancer cells[63]. Interestingly, transcriptomic analysis of breast cancer cells showed that GPR109A activation inhibits genes related to cell survival and anti-apoptotic signaling, identical to our gene sets differentially regulated in GC B cells of mice with kidney disease.

The majority of the studies linked GPR109A to controlling inflammation in various tissues and organs including the gut, vascular wall, CNS, and retina[64]. Most importantly, GPR109A signaling in colonic macrophages and dendritic cells is required to induce immunoregulatory Treg cells and IL-10-producing T cells[51]. Accordingly, *Niacr1*$^{-/-}$ mice exhibit a reduced number of Treg cells in the colon[65]. We also observed increased Treg cells in the spleen of uremic mice during T-dependent immune response, indicating that HA/GPR109A signaling may contribute to the homeostasis and function of Treg cells in kidney disease. This result prompts future studies to define the contribution of various immune cells' specific HA/GPR109A signaling in the generation and function of T regs in uremic mice.

Our data show a similar impairment in GC formation and influenza-specific antibody response, which correlated with diminished pulmonary inflammation and an inability to clear the virus from the lungs of mice with kidney dysfunction. These results have ramifications for other respiratory viruses including SARS-CoV-2 infection, a major clinical problem in patients with kidney disease during the recent pandemic. It is estimated that SARS-CoV-2-related mortality was about ten times higher in patients with kidney disease than those with normal kidney function[4,66]. COVID-19 prevention through successful vaccination is therefore paramount in this vulnerable population. Unfortunately, patients with kidney disease generated poor antibody response following mRNA vaccination against SARS-CoV-2[16]. Thus, understanding the mechanisms by which kidney dysfunction impacts B cell response may shed light on how to generate protective immunity following natural infection or vaccination against SARS-CoV-2 in patients with kidney disease.

Methods

The research described here complies with all relevant ethical regulations. All animal experiments were conducted following the National Institute of Health guidelines under protocols approved by the University of Pittsburgh Institutional Animal Care and Use Committee (Protocol number: 23073326) and Stony Brook University Institutional Animal Care and Use Committee (Protocol number: 2024-00044). All human participants' studies were approved by the University of Pittsburgh Institutional Review Board (IRB number: 19050056).

Mice

μMT (C57BL/6J background: B6.129S2-Ighmtm1Cgn/J; Strain #:002288) mice was purchased from Jackson Laboratories. *Niacr1*$^{-/-}$ mice (C57BL/6J background) was a kind gift from Dr. Thangaraju (Augusta University) and Dr. Offermanns (Max Planck Institute for Heart and Lung Research), as described before[67]. Briefly, the targeting vector was constructed and gene targeting in E14.1 ES cells was performed. Two independently derived ES cell clones were injected into C57BL/6 blastocysts. Germline transmission was confirmed by PCR and Southern blot analysis. Heterozygous mice were back-crossed 5 times into the C57BL/6 strain, and homozygous offspring were obtained by intercrossing *Niacr1*$^{+/-}$ mice. All mice were housed in specific pathogen-free conditions under the supervision of the Division of Laboratory Animal Resources, University of Pittsburgh, and the Division of Laboratory Animal Resources, Stony Brook University. The experimental and control animals were kept separately in the same room at the animal facilities of the University of Pittsburgh and Stony Brook University. All mice were housed under a 12/12 light/dark cycle, 64–79 °F, and 30–70% humidity. All animals were age (8–10 weeks old)- and sex-matched (both male and female) and were randomly assigned. For all experiments, mice were euthanized with CO_2 asphyxiation followed by cervical dislocation.

Immunizations and influenza A virus infection

Eight- to 12-weeks-old WT and *Niacr1*$^{-/-}$ mice were immunized i.p. with 100 μg of 4-Hydroxy-3-nitrophenylacetyl hapten conjugated to Keyhole Limpet Hemocyanin (NP-KLH) (Bioresearch Technologies) precipitated in alum (Thermo Fisher Scientific) and analyzed at day 12 post-immunization. For prime-boost immunization, mice were immunized with NP-KLH in alum followed by a boost with NP-KLH only at day 36 post-immunization. The secondary immune response was measured 6 days post-boost. Eight- to 12-weeks-old WT mice were immunized i.p. with 2.5% SRBC (LAMPIRE Biological Lab) and analyzed at day 7 post-immunization. Eight- to 12-weeks-old WT mice were infected with 1000 PFU of mouse-adapted influenza H1N1 strain A/PR/8/34 via oropharyngeal aspiration, as described before[68].

Mouse model of kidney disease

WT mice were injected i.p. with AAI (7.5 mg/kg b.wt) (Sigma) once. Mice in the non-nephrotoxic control group were i.p. injected with AAII (7.5 mg/kg b.wt) (Sigma) and control animals received a similar volume of PBS[30].

WT mice were operated on for two-stage 5/6 nephrectomy at Charles River Laboratories (Wilmington). Kidney function was assessed by measuring serum BUN using a kit (Bioo Scientific Corp.)[30]. Renal

https://doi.org/10.1038/s41467-024-55187-w

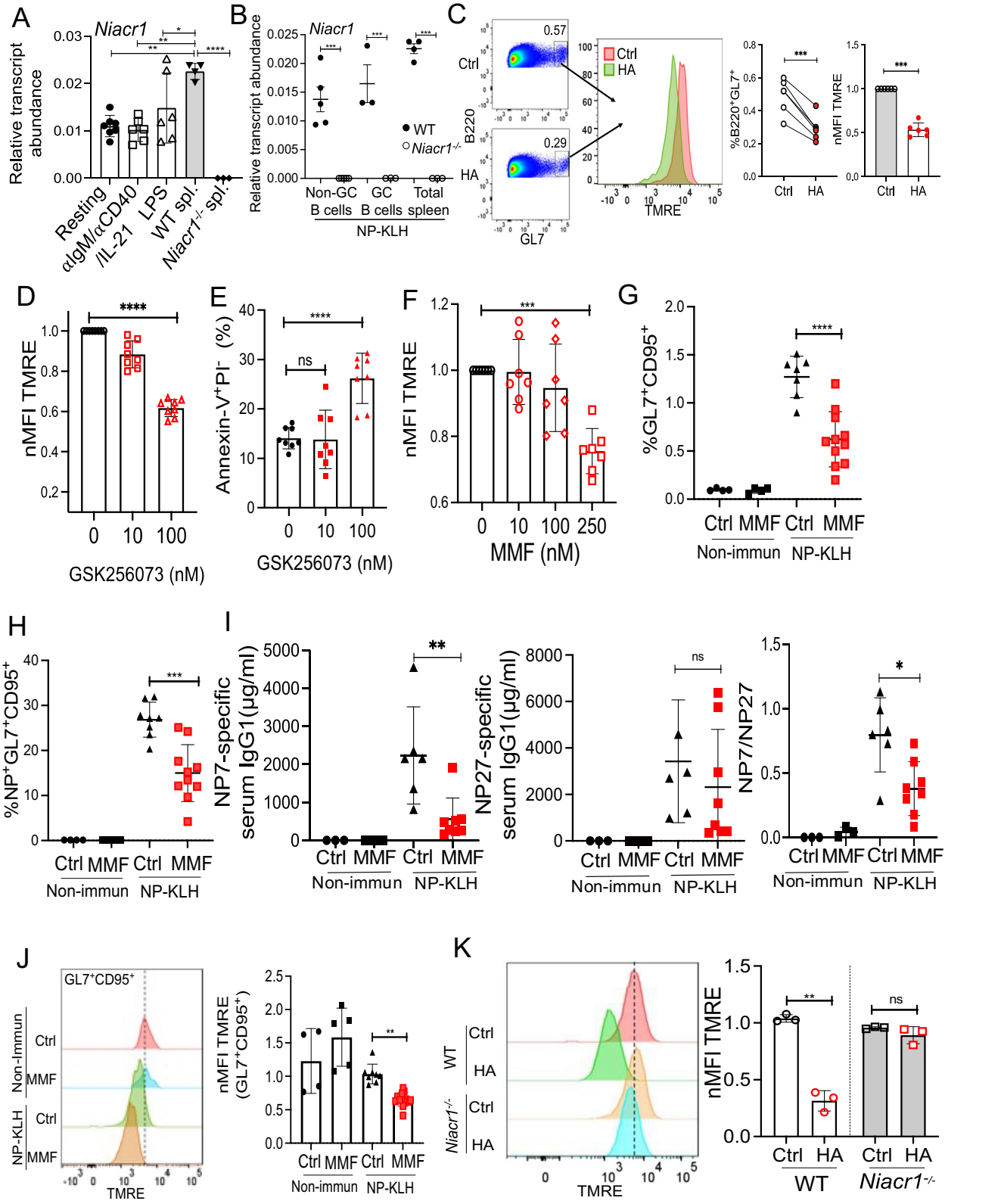

fibrosis was evaluated following staining with Masson's trichrome stain of kidney sections.

Human participants

The blood samples were obtained after providing written informed consent as part of a study entitled "Banking of Biological Samples and Collection of Clinical Data for Connective Tissue Disease" at the Division of Rheumatology and Clinical Immunology, U. Pitt. A written informed consent, which was approved by the University of Pittsburgh Institutional Review Board (IRB number: 19050056), was in place for the human studies. No study participants were compensated. All demographic information is provided in Table S1.

Fig. 6 | HA causes apoptosis of B cells via GPR109A. A Resting splenic B cells ($n = 5–6$) ± αIgM/αCD40/IL-21 or LPS were assessed for *Niacr1* mRNA expression by RT-qPCR at 24 h. Total splenocytes from WT and *Niacr1*$^{-/-}$ mice ($n = 3$) were used as positive and negative controls, respectively. **B** *Niacr1* transcript expression was assessed by RT-qPCR on NP-KLH immunized and FACS-sorted non-GC (liveB220^{+}GL7^{-}CD95^{-}), total GC (liveB220^{+}GL7^{+}CD95^{+}) (2 mice pooled together) and total spleen cells from WT and *Niacr1*$^{-/-}$ mice ($n = 6$) at day 12 post-immunization. **C** Purified total WT B cells from NP-KLH immunized mice (at day 12 post-immunization) were incubated with HA for six hours and assessed for the loss of mitochondrial membrane potential of GC B cells by TMRE staining (B220^{+}GL7^{+}) cells. B cells ± αIgM/αCD40/IL-21± (**D** and **E**) GSK256073/± (**F**) MMF and mitochondrial membrane potential and apoptosis of plasmablasts were measured. Immunized WT mice were i.p. injected with MMF or left untreated (Ctrl) every alternate day and evaluated for **G** total GC [Non-immun: Ctrl (4), MMF (4); NP-KLH: Ctrl (7), MMF (11)], **H** NP-specific GC [Non-immun: Ctrl (4), MMF (4); NP-KLH: Ctrl (7), MMF (11)], **I** serum NP7 and NP27-specific IgG1 titers and affinity maturation (NP7/NP27-IgG1 ratio) [Non-immun: Ctrl (3), MMF (3); NP-KLH: Ctrl (6), MMF (8)] and **J** loss of mitochondrial membrane potential of GC B cells [Non-immun: Ctrl (4), MMF (5); NP-KLH: Ctrl (8), MMF (13)]. **K** Resting splenic B cells ($n = 3$) from WT and *Niacr1*$^{-/-}$ mice were stimulated with αIgM/αCD40/IL-21 in the presence or absence of HA. The B220^{+}CD138^{+} cells were analyzed for the loss of mitochondrial membrane potential by TMRE staining 24 h later. Each dot represents individual mice (**B** and **G**–**J**) and individual experiments (**A**, **C**–**F**, and **K**). Data pooled from 2–3 independent experiments (**B** and **G**–**J**) and individual experiments **A** (5), **C**, **D** (8), **E**, **F** (7) and **K** (3). Data expressed as Mean ± SD. Statistical analyses by One-way ANOVA (**A**, **B**, and **D**–**K**) and two-sided t-test (**C**). **A** Resting vs. WT spleen $^{**}P = 0.0015$, αIgM/αCD40/IL-21 vs. WT spleen $^{**}P = 0.0010$, LPS vs WT spleen $^{*}P = 0.0523$, WT spleen vs. *Niacr1*$^{-/-}$ spleen $^{****}P < 0.0001$. **B** Non-GC B cells $^{***}P = 0.0005$, GC B cells $^{***}P = 0.0004$, Total Spleen $^{***}P = 0.0002$. **C** $^{***}P = 0.0004$ and $^{****}P = 0.0005$. **D** $^{****}P < 0.0001$. **E** $^{****}P < 0.0001$. **F** $^{***}P = 0.0008$. **G** $^{****}P < 0.0001$. **H** $^{***}P = 0.0002$. **I** $^{**}P = 0.0067$ and NP7/NP27: $^{*}P = 0.0106$. **J** $^{**}P = 0.0015$. **K** $^{**}P = 0.0134$. ns: statistically not significant. Source data are provided as a Source Data file.

Cell preparation and in vitro stimulation

Resting splenic B cells and total B cells were purified (>95% purity) by negative selection (Miltenyi Biotech). The B cells were either labeled with CFSE (Invitrogen) or unlabeled and activated with Fab Fragment Goat α-mouse IgM, μ chain specific (10 μg/ml, Jackson Immunoresearch), α-mouse CD40 (5 μg/ml, BD Bioscience) and recombinant IL-21 (50 ng/ml, PeproTech) or LPS (10 μg/ml) in the presence or absence of various uremic toxins [Hippuric acid (HA): 250 μg/ml and 35 μg/ml, Sigma; Urea: 2.3 mg/ml, Sigma; Indole-3-acetic acid (IAA): 10 μM, Sigma; Guanidino acetic acid (GAA): 5 μM, Sigma; Guanidino butyric acid (GBA): 5 μM, Sigma; p-Cresol (PC): 40 μg/ml, Sigma; p-Cresyl sulfate (PCS): 40 μg/ml, APExBio; p-Cresyl glucuronide (PCG): 18 μM, Toronto Research Chemicals Inc.; Indoxyl sulfate (IS): 100 μM, Sigma]. In some experiments, B cells were treated with GSK256073 (TargetMol) and MMF (Sigma)[52,69].

The levels of these uremic toxins in AAN mice serum (as measured by UHPLC MS/MS) are Hippuric acid (HA): 32.7 ± 20.4 μg/ml; Indole-3-acetic acid (IAA): below the limit of detection; Guanidino acetic acid (GAA): 23.6 ± 12.4 μg/ml; Guanidino butyric acid (GBA): below the limit of detection; p-Cresyl sulfate (PCS): 3.7 ± 4.1 μg/ml; p-Cresyl glucuronide (PCG): 2.4 ± 3.1 μg/ml; Indoxyl sulfate (IS): 48.7 ± 16.3 μg/ml (Jawale et al., 2021).

Human B cells were purified from the peripheral blood of healthy donors by negative selection [Miltenyi Biotech (>95% purity)]. B cells were activated with human α-IgM/IgG (10 μg/mL; Jackson Immunoresearch), soluble CD40L (sCD40L) (50 ng/ml, PeproTech), and recombinant IL-21 (50 ng/ml, PeproTech).

Adoptive transfer of B cells

Resting splenic B cells were purified (>95% purity) by negative selection (Miltenyi Biotech) and adoptively transferred into *muMT* mice (10 million cells/mouse) via tail vein injection.

Enzyme-linked immunospot assay (ELISPOT)

To measure IgG or IgM-secreting plasma cells, multiscreen filter 96 well plates (Millipore) were coated overnight at 4 °C with 100 μl/well of NP4 or NP7-BSA, as shown before[70]. The coated plates were blocked with a complete RPMI1640 medium (Corning). One - 0.5 million splenocytes were added in each well in duplicates and incubated overnight at 37 °C and 5% CO_2. The plates were washed with PBS + 0.1% Tween 20 (Sigma) and anti-mouse IgM-HRP or anti-mouse IgG1-HRP antibody (Southern Biotech) were added and incubated overnight at 4 °C. The spots were visualized with AEC substrate (BD Biosciences) for 30 min at room temperature in the dark and reaction was stopped by rinsing plates with distilled water. The membranes were airdried and the spots were counted using the AID Classic ELISPOT reader (AID Autoimmun Diagnostika, GMBH).

Enzyme-linked immunosorbent assay (ELISA)

Serum ELISA was performed to detect IgG and IgM antibody titers, as described before[70]. Briefly, 96 well plates (Nunc) were coated overnight at 4 °C with unlabeled Ig (Southern Biotech), NP4 or NP7-BSA (Bioresearch Technologies) or NP27-BSA (Bioresearch Technologies). The coated plates were blocked with a blocking buffer. Next, 50 μl/well of standard IgG1 or IgM was added in unlabeled Ig-coated wells and diluted serum samples in NP-coated wells and incubated overnight at 4 °C. After washing, 50 μl/well of anti-mouse IgM-HRP or anti-mouse IgG1-HRP antibody (Southern Biotech) were added and incubated for 2 h at room temperature in the dark. The plates were washed several times and developed for 5 min with TMB substrate mix (BioLegend). The reaction was stopped with acid stop solution (BioLegend) and the plates were read in BioTek Synergy H1 Multimode Reader (Agilent). Serum glucocorticoids level was measured at day 12 post-immunization using a commercially available mouse glucocorticoids ELISA kit (MY BioSource.com).

Hemagglutination inhibition assay (HIA)

Anti-influenza hemagglutinin titer was measured from the serum of influenza-infected and uninfected control mice, as shown before[71]. Briefly, one day before the assay all serum samples were pretreated with receptor-destroying enzyme (RDE) from Cholerae Filtrate (Sigma) at 37 °C overnight and then heat-inactivated at 56 °C for 30 min. Anti-influenza hemagglutinin antibody (Antibodies-online Inc) was used as a positive control to inhibit the hemagglutination of 1% Guinea pig red blood cells GRBC (Cederlane) induced by hemagglutinin (Sino Biologicals Inc). An equal volume of standardized viral antigen (4 HA units) was added to each well and the mixture was incubated at room temperature for 30 min. 1% GRBC was added in equal volume to the assay content and left undisturbed for 1 h at room temperature. The plates were evaluated for the presence of agglutination inhibition. The antibody titer was expressed as the reciprocal highest serum dilution that showed complete inhibition of agglutination.

qPCR

The mRNA was isolated from homogenized lung tissues using an RNeasy kit (Qiagen). Complementary DNA was synthesized from the mRNA using SuperScript III reverse transcriptase (Invitrogen) and subjected to qPCR (*Niacr1*) and Taqman qPCR (*Influenza M1*), as previously described[62,68]. Primers for *Niacr1* were obtained from IDT and Qiagen. Primers for *Gapdh* and *Hprt* were obtained from Qiagen.

Niacr1: *5′-GTTACAACTTCAGGTGGCACGAT-3′* (forward);
5′-CTCCACACTAGTGCTTCGGTTATT-3′ (reverse)
Influenza M1: *5′-GGACTGCAGCGTAGACGCTT-3′* (forward);
5′-CATCCTGTTGTATATGAGGCCCAT-3′ (reverse);

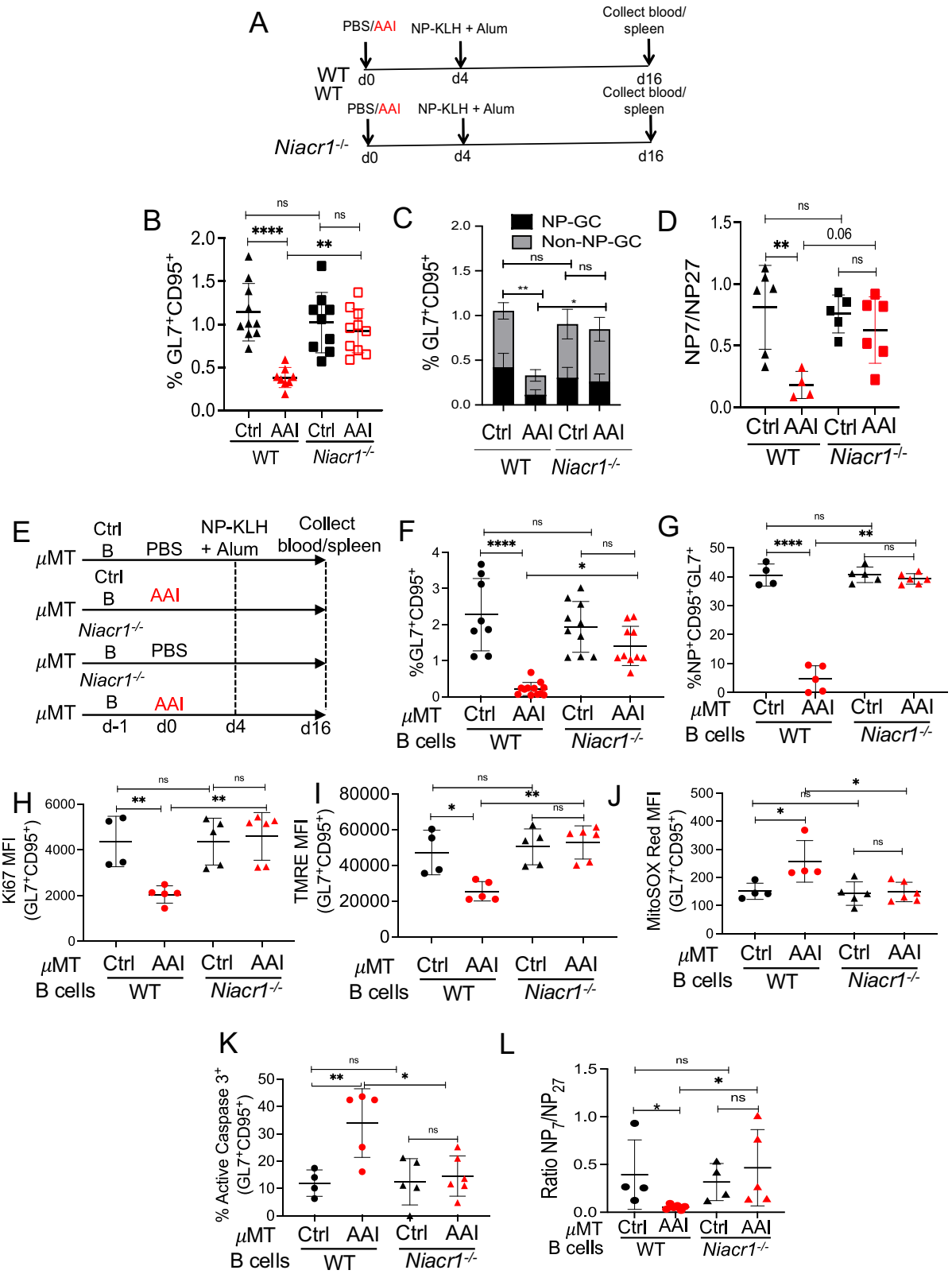

5′-/56-FAM/CTCAGTTAT/ZEN/TCTGCTGGTGCACTTGCCA/ 3IABkFQ/-3′ (FAM probe)

In vivo treatment of mice

Mice were i.p. injected with organic anion transporter 1 and 3 inhibitor Probenecid (Invitrogen) (150 mg/kg b.wt) or vehicle control once on the day of AAI injection[30].

Mice were treated with GPR109A agonist MMF (100 mg/kg b.wt) (Sigma) starting 2 days post-immunization and then every alternate day till day 12 post-immunization[69,72].

Tissue histology and scoring

Lungs and kidneys were fixed in 10% neutral-buffered formalin and embedded in paraffin. Tissue sections were stained with H&E and

Fig. 7 | B cell-specific GPR109A expression induces apoptosis in kidney disease. **A** Diagram of the experimental design. WT and *Niacr1*$^{-/-}$ mice (n = 8–10) were subjected to AAN followed by NP-KLH in alum immunization. **B** Total GC B cells (liveB220^{+}GL7^{+}CD95^{+}) [NP-KLH: WT Ctrl (10), AAI (8); *Niacr1*$^{-/-}$ Ctrl (9), AAI (10)], **C** NP-specific GC B cells (liveB220^{+}NP^{+}GL7^{+}CD95^{+}) by flow cytometry [NP-KLH: WT Ctrl (11), AAI (9); *Niacr1*$^{-/-}$ Ctrl (11), AAI (10)], and **D** antibody affinity maturation as assessed by NP7/NP27-specific serum IgG1 ratio was evaluated at day 12 post-immunization [NP-KLH: WT Ctrl (6), AAI (4); *Niacr1*$^{-/-}$ Ctrl (5), AAI (6)]. **E** Resting splenic B cells from WT or *Niacr1*$^{-/-}$ mice were adoptively transferred into control or AAN μMT mice one day before AAI injection. Mice were immunized with NP-KLH in alum four days post-AAI-injection. At day 12 post-immunization, spleens were assessed for **F** total GC formation [NP-KLH: WT Ctrl (8), AAI (12); *Niacr1*$^{-/-}$ Ctrl (10), AAI (10)], **G** NP-specific GC formation [NP-KLH: WT Ctrl (4), AAI (5); *Niacr1*$^{-/-}$ Ctrl (5), AAI (6)], **H** proliferation [NP-KLH: WT Ctrl (4), AAI (5); *Niacr1*$^{-/-}$ Ctrl (5), AAI (6)], **I** loss of mitochondrial membrane potential [NP-KLH: WT Ctrl (4), AAI (5); *Niacr1*$^{-/-}$ Ctrl (5), AAI (6)], **J** mitochondrial ROS generation by total GC B cells [NP-KLH: WT Ctrl (4), AAI (5); *Niacr1*$^{-/-}$ Ctrl (5), AAI (6)], **K** apoptotic NP-specific GC B cells by flow cytometry [NP-KLH: WT Ctrl (4), AAI (5); *Niacr1*$^{-/-}$ Ctrl (5), AAI (6)], and **L** antibody affinity maturation as assessed by NP7/NP27-specific serum IgG1 ratio [NP-KLH: WT Ctrl (4), AAI (6); *Niacr1*$^{-/-}$ Ctrl (4), AAI (5)]. Each dot represents individual mice (**B**–**D** and **F**–**L**). Data pooled from 2–3 independent experiments (**B**–**D**, and **F**–**L**). Data expressed as Mean ± SD. Statistical analyses by One-way ANOVA (**B**–**D**, and **F**–**L**). **B** WT Ctrl vs AAI ****P < 0.0001, WT AAI vs *Niacr1*$^{-/-}$ AAI **P = 0.0017. **C** WT Ctrl vs AAI **P = 0.005, WT AAI vs *Niacr1*$^{-/-}$ AAI *P = 0.04852. **D** WT Ctrl vs AAI **P = 0.0060. **F** WT Ctrl vs AAI ****P < 0.0001, WT AAI vs *Niacr1*$^{-/-}$ AAI *P = 0.0142. **G** WT Ctrl vs AAI ****P < 0.0001, WT AAI vs *Niacr1*$^{-/-}$ AAI **P = 0.006. **H** WT Ctrl vs AAI **P = 0.0093, WT AAI vs *Niacr1*$^{-/-}$ AAI **P = 0.0018. **I** WT Ctrl vs AAI *P = 0.0162, WT AAI vs *Niacr1*$^{-/-}$ AAI **P = 0.0010. **J** WT Ctrl vs AAI *P = 0.0243, WT AAI vs *Niacr1*$^{-/-}$ AAI *P = 0.0110. **K** WT Ctrl vs AAI **P = 0.0096, WT AAI vs *Niacr1*$^{-/-}$ AAI *P = 0.0115. **L** WT Ctrl vs AAI *P = 0.0653, WT AAI vs *Niacr1*$^{-/-}$ AAI *P = 0.0150. ns: statistically not significant. Source data are provided as a Source Data file.

Masson's Trichome stain, and histological scores were evaluated, as described before[68].

Flow cytometry

Spleens were harvested from mice and subjected to mechanical dissociation to prepare single-cell suspensions, followed by RBC lysis by ACK lysing buffer (Gibco). The following antibodies and reagents were used for surface staining of immune cells: α-B220 (BD Biosciences, Clone: RA3-6B2), α-GL7 (BD Biosciences, Clone: GL7), α-CD95 (Invitrogen, Clone: 15A7), NP (Bioresearch Technologies), α-IgG1 (BD Biosciences, Clone: A85-1), α-CD138 (BD Biosciences, Clone: 281-2), α-CD4 (BioLegend, Clone: GK1.5), α-CD44 (Invitrogen, Clone: IM7), α-CD62L (BD Biosciences, Clone: MEL-14), α-CXCR5 (BioLegend, Clone: L138D7), α-PD-1 (BioLegend, Clone: RMP1-30), α-CD25 (BD Biosciences, Clone: 7D4), α-CXCR4 (Invitrogen, Clone: 2B11), α-CD86 (BioLegend, Clone: GL-1), α-CD8 (BioLegend, Clone: 53-6.7), Ki67 (Invitrogen, Clone: SolA15) and Influenza-specific Tetramer (Influenza A NP 366-374: NIH Tetramer Core Facility). Surface staining of human B cells was performed with human α-GPR109A antibody (Invitrogen, Clone: 4NZBRGO). Dead cells were excluded using the Live/Dead Ghost Dye™ Violet 510 dye (TONBO biosciences). Mitochondrial membrane potential was assessed by Tetramethylrhodamine ethyl esterperchlorate (TMRE) staining (Thermo Fisher Scientific). Mitochondrial ROS was measured by MitoSOX™ Red Mitochondrial Superoxide Indicator (Invitrogen). The percentage of apoptotic B cells was assessed by Annexin-V/PI staining kit (BD Pharmingen). To detect active Caspase3 expression, cells were stained with a CaspGLOW Fluroscein active Caspase3 staining kit (Thermo Fisher Scientific). Cell proliferation was determined by determining the serial dilution of CFSE dye (Invitrogen). For in vivo cell cycle analysis, mice were injected i.p. with bromodeoxyuridine (3 mg/mouse) (BrdU flow kit; BD Biosciences) 6 h before sacrifice. For intracellular staining, LPS (2 μg/ml; Sigma) restimulated B cells were fixed and permeabilized in perm/wash buffer (BD Biosciences) for 30 min on ice. Cells were then stained for 1 h on ice in perm/wash buffer with α-mouse-IL-6 antibody (Invitrogen: Clone MP5-20F3). Foxp3 intracellular staining was performed using a Foxp3 staining kit (eBioscience). Data was acquired with a FACS Fortessa (BD Biosciences) and analyzed using FlowJo (Version: V10.10.0: Tree Star).

Immunofluorescence staining

Frozen sections (7 μm thickness) were fixed in acetone and blocked with 1% BSA in PBS. GC formation was evaluated by staining with fluorescent conjugated α-mouse B220 (BioLegend; Clone RA3-6B2), α-mouse IgD (BioLegend; Clone 11-26c.2a) and α-mouse Bcl6 (BD Biosciences; Clone K112-91) antibodies. Slides were mounted with Vectashield without 4′,6′-diamidino-2-phenylindole (Vector Labs) and images were acquired with EVOS FL Auto microscope (Life Technologies).

Computational analysis of RNA-Seq data

After initial QC and adapter trimming, the sequence data was quantified using Kallisto, to obtain transcript level abundances using mm10 (UCSC) as a reference. Post quantification differentially expressed genes and transcripts between the control and uremic mice GC B cells were identified using Sleuth. We used default sleuth parameters to perform normalization and filtering. Sleuth estimates size factors using the median ratio method, which in turn is used for the normalization of estimated counts. Low abundance transcripts i.e. transcripts with estimated counts less than 5 are removed from further analysis. Finally, the design formula only included one-factor group (~group) with two levels: GC B cells from control and uremic mice. The significant differentially expressed transcripts were defined using a q-value (Benjamini–Hochberg adjusted p-value) threshold of <0.05. Over-representation analysis was performed using the WebGestalt tool to identify the enrichment of the genes in specific pathways described in the Kyoto Encyclopedia of Genes and Genomes (KEGG) and Reactome databases. The LZ and DZ gene lists were manually curated from manuscript search and the genes that showed differential expression in our data were used to generate heatmap.

LC-MS/MS

An ultra-performance liquid chromatography-tandem mass spectrometry (UPLC-MS/MS) system consisting of a Waters Acquity I-class UPLC and Thermo Scientific TSQ Quantis Plus equipped with a heated electrospray ionization source was used. The selected reaction monitoring transitions used for quantitation were m/z 177.9 → 134.0 for hippuric acid and m/z 182.9 → 139.0 for *d5*-hippuric acid. To that end, 50 μL of serum was protein precipitated using 100 μL of acetonitrile containing internal standard. The sample was briefly vortexed and then centrifuged at 10,000 × g for 5 min before the supernatant was transferred and evaporated at 40 °C under nitrogen. The samples were reconstituted with 150 μL of 85:15 (water:acetonitrile, v:v), and 20 μL was injected into the UPLC-MS/MS system. Chromatographic separation of the samples was accomplished with a Waters Acquity BEH C18 (2.1 × 100 mm, 1.7 μm) column with an isocratic elution using 85:15 (A:B, v:v) of 10 mM ammonium formate; pH 4.3 (A) and acetonitrile (B) at a flow rate of 0.3 mL/min.

Statistics and reproducibility

Statistics were conducted using GraphPad Version 7.05.237 software. The following tests were used as indicated in figure legends to determine p-values: ANOVA with Tukey post hoc test, Mann–Whitney, Kruskal–Wallis, and unpaired or paired Student's t-test through GraphPad Prism 7 program. All data are expressed as Mean ± Standard deviation. For all tests, $P < 0.05$ was considered significant (*$0.01 \le P < 0.05$, **$0.001 \le P < 0.01$, ***$0.0001 \le P < 0.001$, ****$P < 0.0001$). At least 2 experimental replicates were performed whenever possible to verify reproducibility. Replicate number is indicated in the figure legends. The experimental groups were randomly assigned. Experimental sample size

https://doi.org/10.1038/s41467-024-55187-w

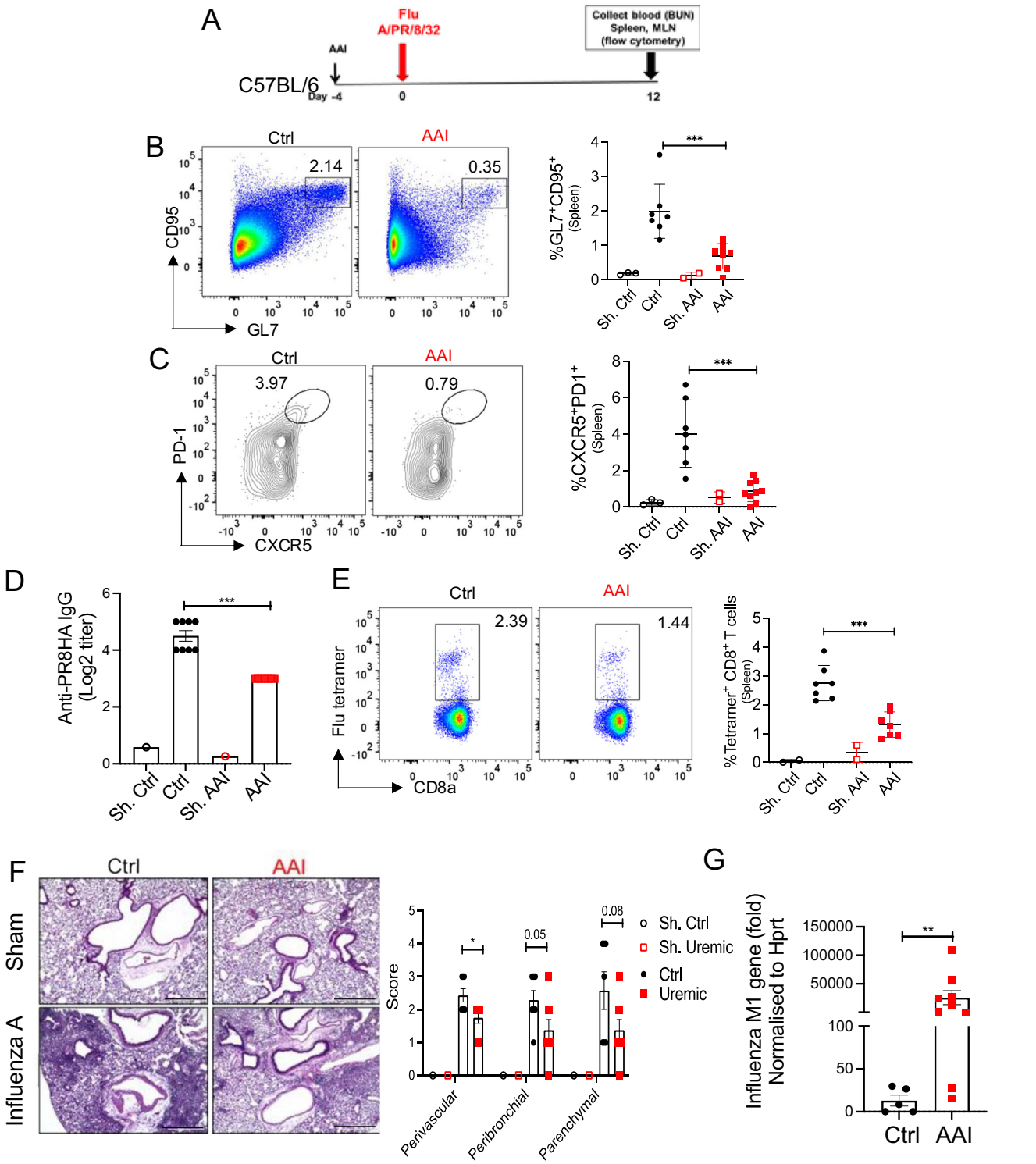

Fig. 8 | Diminished B and T cells response in influenza-infected mice in kidney disease. A Schematic representation of the experimental design. Mice were either injected with AAI or PBS (Ctrl). Four days post-AAI injection, mice were infected with 1000 PFU of mouse-adapted influenza H1N1 strain A/PR/8/34 via oropharyngeal aspiration ($n = 7–9$) or left sham infected ($n = 3$). At day 12 p.i., spleen of infected and sham mice was assessed for **B** GC (liveB220$^+$GL7$^+$CD95$^+$) [Sham: Ctrl (3), AAI (2); Influenza: Ctrl (7), AAI (9)], and **C** TFh (liveCD4$^+$CD44$^+$CXCR5$^+$PD1$^+$) cells by flow cytometry [Sham: Ctrl (3), AAI (2); Influenza: Ctrl (7), AAI (9)], **D** serum anti-PR8HA IgG titer by HAI assay [Sham: Ctrl (1), AAI (1); Influenza: Ctrl (8), AAI (7)], and **E** influenza-specific CD8$^+$ T cells by tetramer staining [Sham: Ctrl (2), AAI (2); Influenza: Ctrl (7), AAI (7)]. **F** Influenza A virus infected and sham lungs were subjected to H&E staining and peri-vascular, peri-bronchiolar, and parenchymal inflammation were scored [Sham: Ctrl (1), AAI (1); Influenza: Ctrl (7), AAI (8)]. Scale bar = 50 µm. **G** Viral load in the lung was quantified by assessing Influenza A virus M1 gene expression by Taqman qPCR assay [Influenza: Ctrl (5), AAI (9)]. Data is normalized to the HPRT gene. Each dot represents individual mice and data are pooled from 2–3 independent experiments (**B**–**G**). Data expressed as Mean ± SD. Statistical analyses by One-way ANOVA (**B**, **C**, and **E**), two-sided t-test (**F**), Mann–Whitney test (**G**), and Kruskal–Wallis test (**D**). **B** ***$P = 0.0007$. **C** ***$P = 0.0003$. **D** ***$P = 0.0002$. **E** ***$P = 0.0005$. **F** Peri-vascular *$P = 0.020521$. **G** **$P = 0.007$. Source data are provided as a Source Data file.

and replicates are indicated in the figure legends. Data points were excluded based on predefined exclusion criteria, only if there were measurement errors, processing errors, poor sampling, or if they were outside of 3-sigma limits. Data acquisition and analysis were performed blind whenever possible.

Reporting summary

Further information on research design is available in the Nature Portfolio Reporting Summary linked to this article.

Data availability

The RNA-seq data generated in this study has been deposited in the GEO (accession code GSE237445) and was made available publicly starting January 1, 2024. The remaining data underlying Figs. 1–8 and Supplementary Figs. are available in the published article and its online supplemental material. Source data are provided with this paper.

References

1. Valderas, J. M., Starfield, B., Sibbald, B., Salisbury, C. & Roland, M. Defining comorbidity: implications for understanding health and health services. *Ann. Fam. Med.* **7**, 357–363 (2009).
2. Gijsen, R. et al. Causes and consequences of comorbidity: a review. *J. Clin. Epidemiol.* **54**, 661–674 (2001).
3. Kovesdy, C. P. Epidemiology of chronic kidney disease: an update 2022. *Kidney Int. Suppl. (2011)* **12**, 7–11 (2022).
4. Mahalingasivam, V. et al. COVID-19 and kidney disease: insights from epidemiology to inform clinical practice. *Nat. Rev. Nephrol.* **18**, 485–498 (2022).
5. Brogan, M. & Ross, M. J. COVID-19 and kidney disease. *Annu Rev. Med* **74**, 1–13 (2023).
6. Allen, C. D., Okada, T. & Cyster, J. G. Germinal-center organization and cellular dynamics. *Immunity* **27**, 190–202 (2007).
7. Cyster, J. G. & Allen, C. D. C. B cell responses: cell interaction dynamics and decisions. *Cell* **177**, 524–540 (2019).
8. Elsner, R. A. & Shlomchik, M. J. Germinal center and extrafollicular B cell responses in vaccination, immunity, and autoimmunity. *Immunity* **53**, 1136–1150 (2020).
9. Shlomchik, M. J., Luo, W. & Weisel, F. Linking signaling and selection in the germinal center. *Immunol. Rev.* **288**, 49–63 (2019).
10. Dobre, M., Meyer, T. W. & Hostetter, T. H. Searching for uremic toxins. *Clin. J. Am. Soc. Nephrol.* **8**, 322–327 (2013).
11. Haddy, F. J., Meyer, T. W. & Hostetter, T. H. Uremia. *N. Engl. J. Med.* **358**, 95 (2008). author reply 95.
12. Vanholder, R. et al. Review on uremic toxins: classification, concentration, and interindividual variability. *Kidney Int.* **63**, 1934–1943 (2003).
13. Vaziri, N. D., Pahl, M. V., Crum, A. & Norris, K. Effect of uremia on structure and function of immune system. *J. Ren. Nutr.* **22**, 149–156 (2012).
14. Syed-Ahmed, M. & Narayanan, M. Immune dysfunction and risk of infection in chronic kidney disease. *Adv. Chronic Kidney Dis.* **26**, 8–15 (2019).
15. Cohen, G. Immune dysfunction in uremia 2020. *Toxins* **12**, 439 (2020).
16. Babel, N., Hugo, C. & Westhoff, T. H. Vaccination in patients with kidney failure: lessons from COVID-19. *Nat. Rev. Nephrol.* **18**, 708–723 (2022).
17. Thieme, C. J. et al. Impaired humoral but substantial cellular immune response to variants of concern B1.1.7 and B.1.351 in hemodialysis patients after vaccination with BNT162b2. *J. Am. Soc. Nephrol.* **32**, 2725–2727 (2021).
18. Grzegorzewska, A. E. Prophylactic vaccinations in chronic kidney disease: current status. *Hum. Vaccin. Immunother.* **11**, 2599–2605 (2015).
19. Pesanti, E. L. Immunologic defects and vaccination in patients with chronic renal failure. *Infect. Dis. Clin. North Am.* **15**, 813–832 (2001).
20. Bouts, A. H. et al. Children with chronic renal failure have reduced numbers of memory B cells. *Clin. Exp. Immunol.* **137**, 589–594 (2004).
21. Degiannis, D. et al. In vitro analysis of B lymphocyte function in uraemia. *Clin. Exp. Immunol.* **70**, 463–470 (1987).
22. Raskova, J. et al. B-cell activation and immunoregulation in end-stage renal disease patients receiving hemodialysis. *Arch. Intern. Med.* **147**, 89–93 (1987).
23. Pahl, M. V. et al. Effect of end-stage renal disease on B-lymphocyte subpopulations, IL-7, BAFF and BAFF receptor expression. *Nephrol. Dial. Transpl.* **25**, 205–212 (2010).
24. Fernández-Fresnedo, G. et al. B lymphopenia in uremia is related to an accelerated in vitro apoptosis and dysregulation of Bcl-2. *Nephrol. Dial. Transpl.* **15**, 502–510 (2000).
25. Lederer, K. et al. Germinal center responses to SARS-CoV-2 mRNA vaccines in healthy and immunocompromised individuals. *Cell* **185**, 1008–1024.e1015 (2022).
26. Zou, G., Liu, H., Lin, K., Zhu, K. & Hsieh, T. C. Trends and outcomes of hospitalized influenza patients with end-stage kidney disease: insights from the National Inpatient Sample 2010-2019. *Cureus* **14**, e24484 (2022).
27. Watanabe, T. Renal complications of seasonal and pandemic influenza A virus infections. *Eur. J. Pediatr.* **172**, 15–22 (2013).
28. Remschmidt, C., Wichmann, O. & Harder, T. Influenza vaccination in patients with end-stage renal disease: systematic review and assessment of quality of evidence related to vaccine efficacy, effectiveness, and safety. *BMC Med.* **12**, 244 (2014).
29. Lam, J. H. & Baumgarth, N. The multifaceted B cell response to influenza virus. *J. Immunol.* **202**, 351–359 (2019).
30. Jawale, C. V. et al. Restoring glucose uptake rescues neutrophil dysfunction and protects against systemic fungal infection in mouse models of kidney disease. *Sci. Transl. Med.* **12**, eaay5691 (2020).
31. Debelle, F. D., Vanherweghem, J. L. & Nortier, J. L. Aristolochic acid nephropathy: a worldwide problem. *Kidney Int.* **74**, 158–169 (2008).
32. Huang, L., Scarpellini, A., Funck, M., Verderio, E. A. & Johnson, T. S. Development of a chronic kidney disease model in C57BL/6 mice with relevance to human pathology. *Nephron Extra* **3**, 12–29 (2013).
33. Urate, S. et al. Aristolochic acid induces renal fibrosis and senescence in mice. *Int J. Mol. Sci.* **22**, 12432 (2021).
34. Navarro Garrido, A. et al. Aristolochic acid-induced nephropathy is attenuated in mice lacking the neutral amino acid transporter B(0)AT1 (Slc6a19). *Am. J. Physiol. Ren. Physiol.* **323**, F455–F467 (2022).
35. Jawale, C. V. et al. Uremia coupled with mucosal damage predisposes mice with kidney disease to systemic infection by commensal Candida albicans. *Immunohorizons* **5**, 16–24 (2021).
36. Arkatkar, T. et al. B cell-derived IL-6 initiates spontaneous germinal center formation during systemic autoimmunity. *J. Exp. Med.* **214**, 3207–3217 (2017).
37. Choi, Y. S., Eto, D., Yang, J. A., Lao, C. & Crotty, S. Cutting edge: STAT1 is required for IL-6-mediated Bcl6 induction for early follicular helper cell differentiation. *J. Immunol.* **190**, 3049–3053 (2013).
38. Eto, D. et al. IL-21 and IL-6 are critical for different aspects of B cell immunity and redundantly induce optimal follicular helper CD4 T Cell (Tfh) differentiation. *PLoS ONE* **6**, e17739 (2011).
39. Papillion, A. et al. Inhibition of IL-2 responsiveness by IL-6 is required for the generation of GC-T(FH) cells. *Sci. Immunol.* **4**, eaaw7636 (2019).
40. Wong, K. A., Harker, J. A., Dolgoter, A., Marooki, N. & Zuniga, E. I. T cell-intrinsic IL-6R signaling is required for optimal ICOS expression and viral control during chronic infection. *J. Immunol.* **203**, 1509–1520 (2019).
41. Eivazi, S. et al. Development of T follicular helper cells and their role in disease and immune system. *Biomed. Pharmacother.* **84**, 1668–1678 (2016).
42. Weber, T. S. Cell cycle-associated CXCR4 expression in germinal center B cells and its implications on affinity maturation. *Front. Immunol.* **9**, 1313 (2018).

43. Bock, F. J. & Tait, S. W. G. Mitochondria as multifaceted regulators of cell death. *Nat. Rev. Mol. Cell Biol.* **21**, 85–100 (2020).
44. Nojima, T. et al. In-vitro derived germinal centre B cells differentially generate memory B or plasma cells in vivo. *Nat. Commun.* **2**, 465 (2011).
45. Adesso, S. et al. The uremic toxin indoxyl sulphate enhances macrophage response to LPS. *PLoS ONE* **8**, e76778 (2013).
46. Lins, P. G. et al. Effect of indole acetic acid administration on the neutrophil functions and oxidative stress from neutrophil, mesenteric lymph node and liver. *Life Sci.* **78**, 564–570 (2006).
47. Hirayama, A., Noronha-Dutra, A. A., Gordge, M. P., Neild, G. H. & Hothersall, J. S. Uremic concentrations of guanidino compounds inhibit neutrophil superoxide production. *Kidney Int. Suppl.* **78**, S89–S92 (2001).
48. Bosco, A. M. et al. Free p-cresol alters neutrophil function in dogs. *Artif. Organs* **40**, 480–488 (2016).
49. Chen, J. R. et al. GPR109A mediates the effects of hippuric acid on regulating osteoclastogenesis and bone resorption in mice. *Commun. Biol.* **4**, 53 (2021).
50. Chai, J. T., Digby, J. E. & Choudhury, R. P. GPR109A and vascular inflammation. *Curr. Atheroscler. Rep.* **15**, 325 (2013).
51. Singh, N. et al. Activation of Gpr109a, receptor for niacin and the commensal metabolite butyrate, suppresses colonic inflammation and carcinogenesis. *Immunity* **40**, 128–139 (2014).
52. Sprecher, D. et al. Discovery and characterization of GSK256073, a non-flushing hydroxy-carboxylic acid receptor 2 (HCA2) agonist. *Eur. J. Pharmacol.* **756**, 1–7 (2015).
53. Berger, A. A. et al. Monomethyl fumarate (MMF, Bafiertam) for the treatment of relapsing forms of multiple sclerosis (MS). *Neurol. Int.* **13**, 207–223 (2021).
54. Meier, P., Dayer, E., Blanc, E. & Wauters, J. P. Early T cell activation correlates with expression of apoptosis markers in patients with end-stage renal disease. *J. Am. Soc. Nephrol.* **13**, 204–212 (2002).
55. Yoon, J. W., Gollapudi, S., Pahl, M. V. & Vaziri, N. D. Naïve and central memory T-cell lymphopenia in end-stage renal disease. *Kidney Int.* **70**, 371–376 (2006).
56. Ticinesi, A., Guerra, A., Nouvenne, A., Meschi, T. & Maggi, S. Disentangling the complexity of nutrition, frailty and gut microbial pathways during aging: a focus on hippuric acid. *Nutrients* **15**, 1138 (2023).
57. Huang, M. et al. The uremic toxin hippurate promotes endothelial dysfunction via the activation of Drp1-mediated mitochondrial fission. *Redox Biol.* **16**, 303–313 (2018).
58. Gong, Y. et al. G protein-coupled receptor 109A maintains the intestinal integrity and protects against ETEC mucosal infection by promoting IgA decretion. *Front. Immunol.* **11**, 583652 (2020).
59. Yoshida, H. et al. The cis-regulatory atlas of the mouse immune system. *Cell* **176**, 897–912.e820 (2019).
60. Kostylina, G., Simon, D., Fey, M. F., Yousefi, S. & Simon, H. U. Neutrophil apoptosis mediated by nicotinic acid receptors (GPR109A). *Cell Death Differ.* **15**, 134–142 (2008).
61. Guo, W. et al. GPR109A controls neutrophil extracellular traps formation and improve early sepsis by regulating ROS/PAD4/Cit-H3 signal axis. *Exp. Hematol. Oncol.* **12**, 15 (2023).
62. Elangovan, S. et al. The niacin/butyrate receptor GPR109A suppresses mammary tumorigenesis by inhibiting cell survival. *Cancer Res* **74**, 1166–1178 (2014).
63. Thangaraju, M. et al. GPR109A is a G-protein-coupled receptor for the bacterial fermentation product butyrate and functions as a tumor suppressor in colon. *Cancer Res.* **69**, 2826–2832 (2009).
64. Taing, K., Chen, L. & Weng, H. R. Emerging roles of GPR109A in regulation of neuroinflammation in neurological diseases and pain. *Neural Regen. Res.* **18**, 763–768 (2023).
65. Sivaprakasam, S., Bhutia, Y. D., Ramachandran, S. & Ganapathy, V. Cell-surface and nuclear receptors in the colon as targets for bacterial metabolites and its relevance to colon health. *Nutrients* **9**, 856 (2017).
66. Geetha, D. et al. Impact of the COVID-19 pandemic on the kidney community: lessons learned and future directions. *Nat. Rev. Nephrol.* **18**, 724–737 (2022).
67. Tunaru, S. et al. PUMA-G and HM74 are receptors for nicotinic acid and mediate its anti-lipolytic effect. *Nat. Med.* **9**, 352–355 (2003).
68. Cipolla, E. M. et al. Heterotypic influenza infections mitigate susceptibility to secondary bacterial infection. *J. Immunol.* **209**, 760–771 (2022).
69. Tang, H., Lu, J. Y., Zheng, X., Yang, Y. & Reagan, J. D. The psoriasis drug monomethylfumarate is a potent nicotinic acid receptor agonist. *Biochem. Biophys. Res. Commun.* **375**, 562–565 (2008).
70. Chen, D. et al. Coupled analysis of transcriptome and BCR mutations reveals role of OXPHOS in affinity maturation. *Nat. Immunol.* **22**, 904–913 (2021).
71. Kaufmann, L. et al. An optimized hemagglutination inhibition (HI) assay to quantify influenza-specific antibody titers. *J. Vis. Exp.* **13**, e55833 (2017).
72. Jiang, D. et al. Monomethyl fumarate protects the retina from light-induced retinopathy. *Invest. Ophthalmol. Vis. Sci.* **60**, 1275–1285 (2019).

Acknowledgements

This work is supported in part by NIH grants AI142354, AI162616, AI159058, and AI181831 to P.S.B., and HL107380 to J.F.A. We thank Dr. Harinder Singh for their comments, suggestions, and editing of the manuscript. We thank Maureen Laffoon for collecting healthy volunteer blood. We also thank Unified Flow Core, the Department of Immunology, and the Health Science Sequencing Core Facility at UPMC Children's Hospital of Pittsburgh for flow cytometry and RNA-sequencing analysis, respectively. We also thank the Pitt Biospecimen Core for processing lung histology as well as the University of Pittsburgh Small Molecule Biomarker Core for mass spectrometry analysis.

Author contributions

D.P., C.V.J, W.C., J.F.A., and P.S.B. designed the experiments; D.P., C.V.J., W.C., H.R., D.A., D.L., S.W., G.M.V., and R.W. carried out the experiments; D.P., C.V.J., I.M., T.D.N., J.D., J.F.A., and P.S.B. analyzed the data; M.T. provided research tools; D.P., C.V.J., W.C., and P.S.B. wrote the manuscript.

Competing interests

The authors declare no competing interests.

Additional information

Supplementary information The online version contains supplementary material available at https://doi.org/10.1038/s41467-024-55187-w.

Correspondence and requests for materials should be addressed to Partha S. Biswas.

Peer review information *Nature Communications* thanks Kristin Fenton and the other, anonymous, reviewer(s) for their contribution to the peer review of this work. A peer review file is available.

Reprints and permissions information is available at http://www.nature.com/reprints

Publisher's note Springer Nature remains neutral with regard to jurisdictional claims in published maps and institutional affiliations.

Open Access This article is licensed under a Creative Commons Attribution-NonCommercial-NoDerivatives 4.0 International License, which permits any non-commercial use, sharing, distribution and reproduction in any medium or format, as long as you give appropriate credit to the original author(s) and the source, provide a link to the Creative Commons licence, and indicate if you modified the licensed material. You do not have permission under this licence to share adapted material derived from this article or parts of it. The images or other third party material in this article are included in the article's Creative Commons licence, unless indicated otherwise in a credit line to the material. If material is not included in the article's Creative Commons licence and your intended use is not permitted by statutory regulation or exceeds the permitted use, you will need to obtain permission directly from the copyright holder. To view a copy of this licence, visit http://creativecommons.org/licenses/by-nc-nd/4.0/.

© The Author(s) 2024